

POLITECNICO DI TORINO

Corso di Laurea Magistrale
in Ingegneria Meccanica (Mechanical Engineering)

Tesi di Laurea Magistrale

3D PolyJet Printed Microfluidic Mixer



Relatore

prof. Pietro Asinari

Candidato

Matteo Tamone

Luglio 2018

ACKNOWLEDGMENTS

Sincere appreciation goes to Professor Pietro Asinari, who introduced me to the field of advanced engineering thermodynamics.

I would like to express my gratitude to my Advisor, Professor Jie Xu, who allowed me to develop a research in a fascinating and challenging topic.

I would also like to thank Dr. Méance for all the support and suggestions he gave me during my research, his help was crucial to the development of my project.

Genuine gratitude goes to my family, without whose support I would have not been able to undertake this career.

Finally, I want to thank all the people in the microfluidic lab, which helped to create a great and stimulating work environment.

MT

TABLE OF CONTENTS

<u>CHAPTER</u>		<u>PAGE</u>
1	INTRODUCTION	1
1.1	Active mixing and acoustic microstreaming	3
1.2	Review on 3D printed mixers	7
2	METHODS AND MATERIALS	9
2.1	Overview on 3D printing	10
2.1.1	Stereolithography	11
2.1.2	Material Jetting	12
2.2	Materials	14
3	MIXER DESIGN	17
3.1	Design features and technological limitations	17
3.2	Design specifications	21
3.2.1	Basic design	21
3.2.2	Sidewalls hemispheres design	26
3.2.3	Lateral channels design	31
3.2.4	Design considerations	34
4	RESULTS AND DISCUSSIONS	35
4.1	Experimental setup	35
4.2	Laminar flow and microstreaming	38
4.3	Mixing performance	45
4.4	Results	47
4.4.1	Basic Design	47
4.4.2	Sidewall hemispheres design	55
4.4.3	Lateral channels design	58
4.4.4	Design comparison	66
4.4.5	Final remarks and considerations	68
5	CONCLUSION	71
	APPENDICES	73
	Appendix A	74
	Appendix B	76
	Appendix C	78
	Appendix D	80
	Appendix E	82

TABLE OF CONTENTS (continued)

<u>CHAPTER</u>	<u>PAGE</u>
CITED LITERATURE	83
VITA	89

LIST OF TABLES

<u>TABLE</u>		<u>PAGE</u>
I	THERMOMECHANICAL PROPERTIES RGD837 AND RGD810	15

LIST OF FIGURES

<u>FIGURE</u>		<u>PAGE</u>
1	Laminar flow in microchannel. Notice the laminar patter still present after flow obstructions (1 to 4).	2
2	Microstreaming due to the oscillation of a bubble trapped into a microchannel. 10x magnification. Standard design, $4.8\mu\text{m}$ beads. . .	6
3	Microstreaming pattern as developed by an oscillating bubble. Device manufactured with clear, optically transparent resin.	7
4	Design concept: active mixer incorporating throughout holes open to the atmosphere to allow for liquid-air interface development.	18
5	Mixer design concept, 3D CAD isometric view. Notice holes on top surface. (a) Prototype version. (b) Final design.	22
6	Microfluidic mixer, basic design, VeroWhite. (a) Bottom view. (b) Top view.	23
7	Microfluidic mixer, basic design. (a) CAD model first design, vertical inlets. (b) CAD model second design. (c) Second design, 3D printed, top side. (c) Second design, 3D printed, bottom side.	24
8	Microfluidic mixer, basic design, final version, clear resin. (a) Top view. (b) Bottom view.	25
9	Sidewalls hemispheres design. Extruded $\varnothing 200\mu\text{m}$ hemispheres are centered between holes on the lateral walls of the main channel. First prototype CAD design.	26
10	3D CAD bottom view (prototype version) for the sidewalls hemispheres design. Notice hemispheres (in black) position on lateral walls.	27
11	Microscope imagine of 3D printed micromixer, VeroWhite resin. Notice defects in hemisphere printing on the top wall and support resin still filled in holes (black material inside circular structures).	28
12	Hemispherical design, clear resin, 4x microscope view of the internal channel.	29
13	Microfluidic mixer, sidewalls hemispheres design, final version, clear resin. (a) Top view. (b) Bottom view.	30
14	Design concept for an active mixer derived from the basic design. Channels are cut on both sides of the main microchannel.	31
15	Microfluidic mixer, sidewalls channels, VeroClear. (a) Top view. (b) Bottom view.	32
16	Microfluidic mixer, sidewalls channels, VeroClear. (a) Top view. (b) Bottom view.	33
17	3D printed channel, in the original design a series of top holes with $150\mu\text{m}$ wide diameter were present, but the machine was not able to reproduce the feature.	34

LIST OF FIGURES (continued)

<u>FIGURE</u>		<u>PAGE</u>
18	Experimental setup, schematic view. 1- Syringe pump. 2- Amplifier. 3- Function generator. 4- Microscope. 5- Piezoelectric transducer. 6- Mixer.	36
19	Experimental setup, lab equipment. 1- Syringe pump. 2- Amplifier. 3- Function generator. 4- Microscope. 5- Piezoelectric transducer. 6- Mixer.	37
20	Laminar flow patten, basic mixer design, white resin prototype. 4x magnification.	39
21	Laminar flow patten, basic design, clear resin. 4.8 μ m fluorescent beads.	40
22	Microstreaming patterns around three consecutive holes, basic mixer design. 10x enlargement. (a) 5 frames composition. (b) 10 frames composition. (c) 200 frames composition.	41
23	Microstreaming patterns, basic design, 20x magnification.	42
24	Microstreaming patterns, design with hemispherical features on sidewalls. Notice incompletely developed bubble on the left and the hemispheres. 10x magnification.	43
25	Microstreaming patterns around three consecutive holes, sidewall hemispheres design. 10x enlargement. (a) 5 frames composition. (b) 10 frames composition.	44
26	Section of interest, basic design, VeroClear resin.	48
27	Mixing index at 47 kHz and 20 μ l/min.	48
28	Cross section of interest, basic design, VeroClear resin.	50
29	Mixing index at 47 kHz and 20Vpp.	50
30	Sections of interest, case relating number of holes and RMI.	51
31	Relation between mixing index and number of holes at 450ms.	52
32	Convergence of RMI for basic mixer design.	53
33	Mixing homogeneity through a generic cross section.	54
34	Section of interest, sidewall hemispheres design, constant flow rate.	55
35	Mixing index as function of applied peak to peak voltage, sidewalls hemispheres design.	56
36	Section of interest, sidewall hemispheres design, constant peak to peak voltage.	57
37	Mixing index as function of applied flow rate, sidewalls hemispheres design.	58
38	Microstreaming patterns in sidewalls channels along different portion of a main microchannel. 20x enlargement. (a) 30 frames composition. (b) 30 frames composition. (c) 100 frames composition.	60
39	Section of interest, lateral channels design, constant flow rate. Notice section '1', which is used as reference to measure the dimension of a generic lateral channel.	61
40	Mixing index as function of applied peak to peak voltage, lateral channels design.	62

LIST OF FIGURES (continued)

<u>FIGURE</u>		<u>PAGE</u>
41	Mixing index as function of applied flow rate, lateral channels design.	63
42	Cross section selected to evaluate RMI, case constant applied Vpp, lateral channels design.	64
43	Convergence of relative mixing index, lateral channels design.	65
44	Lateral channels mixer. (a) Leakages in lateral channels. (b) Channels without leakages.	66
45	The picture show as the first hole in all batches for all 3 design has a very low dimensional accuracy.	68
46	Example of image analysis report from ImageJ. 20 frames are extracted to calculate the RMI, as seen in column A. Column B indicates the name of the saved video file, while column C to I give information on the selected cross section at the frame indicated under 'Slice'.	82

LIST OF ABBREVIATIONS

CAD	Computer-Aided Design
DI	Deionized
FEM	Finite Element Method
FPS	Frames Per Seconds
IPA	Isopropyl Alcohol
MJ	Material Jetting
PDMS	Polydimethylsiloxane
RMI	Relative Mixing Index
SLA	Stereolithography
2PP	Two Photon Polymerization
UIC	University of Illinois at Chicago
UV	Ultraviolet
V _{pp}	Voltage Peak-to-Peak

SUMMARY

Mixing is one of the most important challenges in microfluidic systems. Many applications in fields ranging from biomedical engineering to food analysis and chemical synthesis rely on fast and homogeneous mixing at the microscale level. Nevertheless, due to the low Reynolds number associated with microchannels, the flow in microfluidic devices is laminar. Development of fast, inexpensive and reliable micromixers is indispensable, however most of microfluidic components are still produced using traditional soft lithography and molding technologies, which do not allow for fully three dimensional structures, high production throughputs and fast point of care manufacturing. An increasing interest in 3D printing has led various research groups to investigate the feasibility of layer by layer manufacturing for microfluidics. 3D printing potentially permits to fabricate complex shapes in a single production step, while maintaining low costs and high design flexibility. Moreover, 3D printing allows for rapid prototyping and shifting manufacturing directly to the final user. A concept of a new completely 3D printed active micromixer is presented and investigated. Three different devices are manufactured by PolyJet technology, which is capable of producing parts ranging from transparent plastic to biocompatible materials. Different designs are presented to show the high flexibility of 3D printing and its versatility in microfluidics. Homogeneous mixing is demonstrated for all the different mixers, along with the main advantages of the selected technology.

SOMMARIO

La necessità di dover controllare e manipolare con precisione e a costo contenuto piccole quantità di fluidi ha permesso un rapido sviluppo di una recente branca della scienza conosciuta come microfluidica. I sistemi microfluidici trovano applicazioni in vari ambiti, principalmente essi vengono impiegati nella ricerca biomedica e nell'industria chimica ed alimentare. In molte di queste applicazioni è indispensabile essere in grado di miscelare tra di loro due correnti fluide aventi portate molto basse, nell'ordine di alcune decine di microlitri al minuto. Suddetti processi richiedono l'uso di canali di dimensioni estremamente ridotte, sostanzialmente di decine o centinaia di micrometri. All'interno di queste strutture il flusso si sviluppa secondo un regime laminare caratterizzato da numeri di Reynolds estremamente bassi, non di rado inferiori all'unità. In tali condizioni, l'assenza di fenomeni di instabilità e turbolenza risulta estremamente sfavorevole alla miscelazione di due fluidi. L'unico fenomeno fisico utile a tale scopo è la diffusione, processo estremamente lento e poco efficiente, non adatto a soddisfare le tempistiche richieste in ambito industriale. Lo sviluppo di efficienti tecnologie per ottenere una rapida ed omogenea miscelazione di due o più correnti fluide risulta pertanto essere una delle maggiori sfide in campo microfluidico. A questo fine, nel corso degli ultimi decenni, è stata sviluppata una classe di apparecchi, conosciuti come micromiscelatori (micromixers), progettati per promuovere e velocizzare fenomeni diffusivi e di avvezione caotica, tali da indurre in brevissimo tempo una rapida ed efficace miscelazione. Come per la maggior parte dei dispositivi microfluidici, i micromiscelatori vengono generalmente prodotti attraverso

SOMMARIO (continua)

tradizionali tecniche di litografia (soft lithography), le quali, benché economiche, non permettono lo sviluppo di strutture completamente tridimensionali, alta produttività e la possibilità di produrre l'apparecchiatura direttamente nel luogo in cui deve essere utilizzata (point-of-care manufacturing). Un crescente sviluppo e diffusione delle tecnologie di stampa in 3D ha posto le basi per la nascita di uno spiccato interesse verso l'utilizzo di tali sistemi di produzione in campo microfluidico. Sebbene la stampa in 3D risulti ancora essere una tecnologia in fase di sviluppo, essa ha le potenzialità per diventare in un prossimo futuro una valida alternativa ai tradizionali sistemi di produzione attualmente in uso in microfluidica. Idealmente la stampa 3D permette di produrre complesse strutture tridimensionali in un singolo step di lavorazione, allargando notevolmente la quantità di design idonei per applicazioni microfluidiche. Inoltre essa permette notevoli volumi produttivi, bassi costi, alta flessibilità di progetto e consente di spostare la produzione direttamente all'utente finale. Non si dimentichi inoltre che con tale tecnologia è possibile sviluppare rapidamente vari prototipi e testarne le prestazioni.

Il seguente lavoro di ricerca è incentrato sullo sviluppo e produzione di un micromiscelatore tramite stampa 3D. Per tale apparecchiatura è stata scelta una configurazione attiva, ovvero la miscelazione delle correnti fluide avviene tramite l'induzione di perturbazioni all'interno del fluido stesso generate avvalendosi di campi esterni. In particolare l'attuazione del dispositivo avviene tramite onde acustiche prodotte da un trasduttore piezoelettrico. Brevemente, tali onde vengono sfruttate al fine di produrre l'oscillazione di un'interfaccia aria-liquido, generalmente una bolla, la quale si comporta come un attuatore. L'oscillazione comporta lo sviluppo di forze di attrito, le quali a loro volta inducono fluttuazioni di velocità e pressione nel liquido

SOMMARIO (continua)

circostante la bolla stessa. L'effetto così descritto prende il nome di microstreaming. Esso induce perturbazioni nel deflusso tali da promuovere il trasporto di massa e la miscelazione tra correnti fluide. L'intensità del fenomeno è attribuita alle caratteristiche dell'onda acustica generata (ampiezza, frequenza, forma) e dalle caratteristiche di risonanza dell'interfaccia aria-fluido. Un miscelatore progettato basandosi su questa tecnologia risulta essere controllabile e attivabile a piacimento. L'interesse della ricerca è quello di valutare sperimentalmente come un dispositivo di questo genere possa essere stampato in 3D, quali siano le sue prestazioni e quali siano i benefici e le limitazioni dell'utilizzo di questo sistema di produzione rispetto alle tradizionali tecniche di litografia.

Dopo una breve sequenza introduttiva, in cui vengono presentate le motivazioni per la seguente ricerca, l'attuale stato dell'arte della tecnologia di micromiscelazione e il fenomeno fisico del microstreaming, l'attenzione viene focalizzata sulla scelta della più adatta tra le tecnologie di stampa 3D al fine di produrre componenti microfluidici. Segue una lunga sezione relativa alla progettazione del micromiscelatore stesso, contenente informazioni sul ragionamento che ha portato allo sviluppo del primo componente e delle problematiche che ne hanno condizionato lo sviluppo successivo. I relativi capitoli presentano tre diversi modelli di micromiscelatore basati sullo stesso design iniziale e il perché di tale scelta. Il lavoro prosegue illustrando il setup di laboratorio e le prove sperimentali effettuate al fine di valutare le prestazioni dei componenti realizzati tramite stampa in 3D. In particolare, un parametro, il Relative Mixing Index (RMI), è stato scelto per analizzare quantitativamente i dati provenienti dai test eseguiti e confrontare tra di loro i vari miscelatori. Infine vi è posta attenzione sui risultati ottenuti,

SOMMARIO (continua)

sulle problematiche sorte durante lo sviluppo e la produzione dei componenti, sui vantaggi della tecnologia adottata e sulle limitazioni che essa pone allo stato attuale dell'arte.

Le prove condotte hanno dimostrato come la tecnologia di stampa 3D PolyJet abbia le caratteristiche necessarie per produrre semplici micromiscelatori attivi con ampia flessibilità di progettazione. Nel contempo si è anche dimostrato come tale tecnologia ponga ancora dei limiti dovuti all'estrema accuratezza e precisione necessarie in microfluidica. Ciò suggerisce che la stampa 3D sia utile da affiancarsi alle tecniche tradizionali di litografia, senza però prendervi il posto. Il livello di miscelazione ottenuto è omogeneo e rapido, tuttavia i dispositivi sono in grado di manipolare portate estremamente basse e i difetti di stampa influenzano notevolmente le loro prestazioni. Ciò nonostante è auspicabile che in un prossimo futuro, l'introduzione di stampanti di nuova generazione e formulazioni innovative di materiali per la stampa 3D consentano in breve tempo di colmare il divario con le tecnologie di produzione tradizionali attualmente in uso. Se tali prospettive verranno rispettate, l'utilizzo della stampa 3D potrebbe rivoluzionare la microfluidica, rendendo i suoi dispositivi fruibili a chiunque abbia a disposizione una stampante 3D.

CHAPTER 1

INTRODUCTION

Microfluidic technologies have become essential in many fields, including biomedical engineering, chemical synthesis, drug development and food analysis. Microscale devices allow to drastically increase the surface to volume ratio of the implemented channels, a characteristic advantageous for many applications, such as biosensing, sample dilution and reagents mixing [1] [2] [3]. At the same time, many of these applications rely on fast and homogeneous mixing to obtain a cost effective, rapid process. However, due to the extremely low Reynolds number regimens associated with microfluidic components, the flow nature in microscale channels is laminar [4]. The Reynolds number expresses the ratio between inertial and viscous forces, in many microfluidics applications it can be smaller than one [3]. A low Reynolds number denotes the predominance of viscous forces, an effect explainable considering the small features and low fluid velocities involved in microfluidics. As a result, the flow at these regimes is laminar. Turbulence and instabilities, responsible for mixing at the macroscopic scale, are not present. Molecular diffusion plays the dominant role for microscale mixing, but it is an inherently slow process, not useful for practical applications in which fast and homogeneous mixing is required. To enhance the process different mixing schemes and technologies have been developed: the basic idea is to prompt convective phenomena by external forces or by shaping complex microchannels internal architectures to increase the contact area, or the contact time, between the fluids to be mixed [1]. Flow laminarity in microchannels is shown in figure Figure 1, at a low Reynolds

number (0.74) two fluids tend to resist mixing even if their path is obstructed. The image has been obtained by 3D printing a microfluidic device consisting of two inlets and a main channel containing four flow obstructing obstacles.

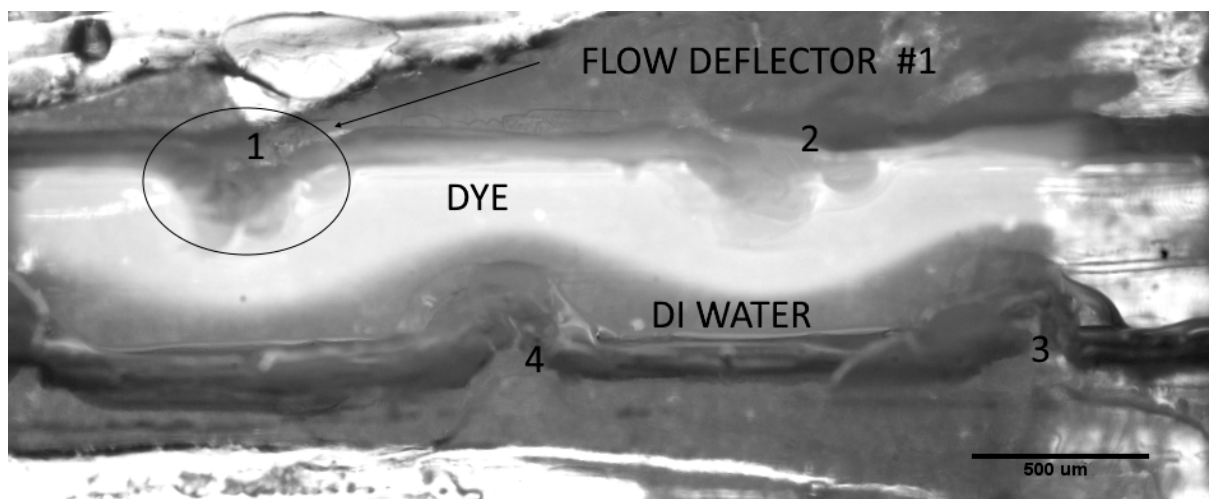


Figure 1: Laminar flow in microchannel. Notice the laminar pattern still present after flow obstructions (1 to 4).

Devices meant for mixing enhancements are usually manufactured by soft lithography and PDMS molding [5]. Nevertheless, soft lithography poses strong design limits: truly three dimensional structures can not be fabricated and PDMS molding is an inherently labor intensive, low throughputs process[5]. At the same time, PDMS devices are also difficult to be integrated in complex assemblies and interfacing with standard industrial fittings is hard [6]. Change in design are feasible only producing a new mask, thus making rapid prototyping laborious and

time consuming. To solve these issues, new manufacturing methods have been investigated, being 3D printing the more promising. Additive manufacturing technologies permit to overcome many of the soft lithography limitations, allowing the design of more complex, truly three dimensional structures in less time and higher production volumes. The main advantages of 3D printing is inherent to the manufacturing process itself, with the opportunity to design intricate 3D architectures in a single step process; this characteristic could in particular revolutionize the microfluidic field, enabling researchers to quickly print and test different designs and allowing point of care manufacturing. New mixing architectures could potentially be developed by exploiting the fully three dimensional capabilities of 3D printing, furthermore classic mixer designs could be enhanced and fabricated in less time and higher throughputs. Mixing modules could be directly incorporated in assemblies or easily interfaced to existing devices by means of standard industrial fittings (threads), which are usually impossible to be implemented in PDMS structures.

1.1 Active mixing and acoustic microstreaming

Microfluidic mixers could be divided in two classes: passive and active mixers. Passive micromixers are mainly designed to increase the contact area between two liquids (lamination-based), enhancing the diffusion process at low Reynolds number regimes [7]. A second common approach consists in the continuous splitting, stretching, folding and recombination of the fluids to generate chaotic advection effects [8]. Examples of passive micromixers are multilamination mixers [9], T-shaped [10] and Y-shaped channels mixers [11], sharp corner micromixers [1] and devices presenting features inside the channels to enhance change in the flow direction

and thus increasing the interaction surface between the fluids [2]. Active micromixers, on the contrary, exploit external force fields (magnetic, acoustic, electric, temperature) [2] and moving components to produce chaotic advection and enhance mixing [7]. Examples of this class of mixers are periodic flow switching devices [12], piezoelectric vibrating membranes [13], magnetic activated microstirrers [14], periodic fluid pulsation devices [12] and acoustically driven bubble-based mixers [15]. Generally passive elements are easier to fabricate, since there is no need to design moving parts or bubble-trapping features, nevertheless user control is very poor and devices can not be switched on/off on demand [4]. On the contrary, active mixers are user controllable, but it comes at the cost of increased complexity in the system [4]. Moreover, heat dissipated by Joule effect in active schemes could pose issues for some chemical reactions [3].

An active, acoustically actuated design has been chosen for this project. 3D printing has been chosen as manufacturing technology. The reasons for these choices are twofold, first active mixing allows for greater user flexibility which is particularly interesting associated with 3D printing: design variations could be quickly done and tested by means of additive manufacturing. Secondly, literature already reports cases of 3D printed passive devices [16] [17] [18], while little testing has been done on active mixing schemes. Eventually, acoustically actuated devices are easy to operate and permit to manipulate the flow contactlessly [19]. In bubble based acoustic devices, mixing is obtained by inducing chaotic advection by means of bubbles oscillations. Acoustically driven vibrating bubbles can show both a linear and unlinear behaviour. They behave like a linear system for low amplitude, stable, motion (non-inertial cavitation). On the contrary, when vibration amplitude drastically increases, bubbles could

undergo violent expansions and contractions, leading to their collapse, a phenomenon known as inertial cavitation, which could be very pernicious for the system structural integrity[20]. When coupled with an acoustic wave of the correct frequency, a linear bubble oscillates and behaves as an actuator, producing frictional forces. These forces are responsible for the development of pressure and velocity fluctuation in the surrounding bulk fluid, which in turn produce a phenomenon known as acoustic microstreaming or cavitation microstreaming [15] [21]. From a theoretical point of view, microstreaming has been described by Hashmi et al. [20] as "a second order non-linear dynamical system" which "exists owing to a difference (phase-shift) between the radial expansion and contraction of a bubble and its translational motion". Microstreaming introduces disturbances in the fluid, which enhance the mass transport and yield in a fast and homogeneous mixing of two fluids. The degree of oscillation of the bubbles is mainly determined by their resonance behavior, which is in turn influenced by their radius. A strong disturbance in the fluid around the bubble is detected when the acoustic wave produced by a piezoelectric transducer meets the resonant frequency of the bubble. Variable flow patterns can be induced around the bubble by exciting the liquid-air interface close to resonance and varying the signal amplitude [22]. The phenomenon can be exploited to produce fast and homogeneous mixing in a channel. It is generally achieved by trapping microbubbles in sidewall, symmetrical, pre-fabricated grooves [23]. It has been proved acoustic actuation can also be exploited to induced pumping [24] [25] and object manipulation [22]. A visualization of microstreaming as induced by a vibrating bubble is show in Figure 2. $4.8\mu\text{m}$ beads have been used to track the fluid pattern around the indicated bubble.

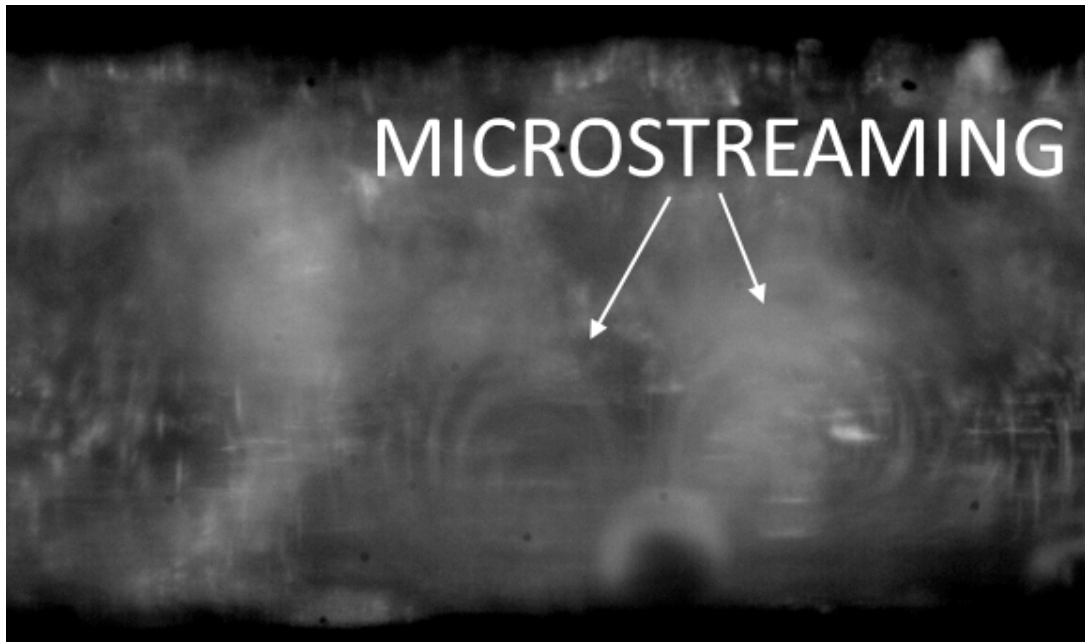


Figure 2: Microstreaming due to the oscillation of a bubble trapped into a microchannel. 10x magnification. Standard design, $4.8\mu\text{m}$ beads.

Another view of a microstreaming pattern can be seen in Figure 3, where beads trajectories around an oscillating bubble are shown. Notice how microstreaming induces a symmetrical, wings-like arrangement of beads. The shown bubble inside the channel is ideally unwanted, nevertheless it illustrates very clearly the bubble ability to develop disturbances in an originally perfectly laminar (DI water and DI water+beads) flow. Moreover, the bubble itself has a contribute to the total mixing performance of the system. It has to be noted that the outcome of acoustically driven microstreaming is very hard to predict using theoretical analysis [19], thus many devices are produced with a trial and error methodology. Due to its inherent versatility, 3D printing could be used for rapid prototyping of many microfluidic devices.



Figure 3: Microstreaming pattern as developed by an oscillating bubble. Device manufactured with clear, optically transparent resin.

1.2 Review on 3D printed mixers

Although 3D printing has been principally used to manufacture passive micromixers, it is interesting to present a brief overview on the principal studies conducted so far on the feasibility of 3D printed micromixers. A more detailed, extensive review of 3D printing technologies and their pro\cons is given in chapter 2.

The first 3D printed microfluidic mixer was developed at the beginning of the 2000 [26], by exploiting a custom made SLA printer developed for university research. The idea was to induce multiple fluid splittings and recombination by means of a complex 3D architecture. In 2010 PolyJet technology has been exploited to design a microfluidic device integrating a passive mixer, in which mixing is induced by appropriately shaped channels [27]. A 3D printed Y-shaped mixer has been obtained in 2015 by means of fused filament fabrication printing, showing the

applicability of a low cost printing technology to the production of simple devices that do not require high printing accuracy (800x800 μ m channels) [28]. Single step manufacturing of transparent 3D printed microfluidic devices (passive mixers, droplet generators and gradient generators) by stereolithography has been investigated by Shallan et al [29]. Modular 3D printed mixers, which consist of simple blocks that can be assembled together, have also been proposed in the last five years [18] [30] [31]. All researches presented in this section give particular emphasis to the 3D printed capability to single step manufacture custom made mixers for rapid prototyping. Lego[®]-like 3D printed blocks could potentially be of great interest, since a standard components library could be developed, moreover the same piece could be used for many applications.

CHAPTER 2

METHODS AND MATERIALS

Microfluidics has long relied on soft lithography as the key technology to produce devices for precise flow control and manipulation. The reasons for its widespread use have to be found in the easiness of SU-8 masters fabrication for PDMS molding and the possibility to reproduce with high accuracy sub millimeter features, such as cavities, channels and holes. PDMS still remains the most used material for microfluidics [6] ensuring biocompatibility, low toxicity, inertness, low cost, optical transparency and elasticity [32]. Nevertheless traditional lithography enables only for small throughputs, planar (2D) designs and requires trained personnel for device manufacturing. Moreover interfaces for external equipment and connectors for assembly purposes need to be punched into PDMS, producing non standardized inlets and outlets that are prone to leakages. Eventually PDMS molding is not able to effectively satisfy the need of high throughput point-of-care manufacturing that is becoming prominent in various scientific and industrial fields [6]. To solve these issues and permit further developments in microfluidics, 3D printing has been proposed as a possible new manufacturing process for microfluidic devices. Scientific citations of the keyword '3D printing' associated with microfluidic research have exponentially increased in the past couple of years, thus indicating an high potential and interest in this technology [6].

2.1 Overview on 3D printing

3D printing commonly refers to a series of manufacturing technologies which permit to obtain three dimensional structures by sequential, layer by layer, material solidification or joining [33]. Development of the first 3D printing process dates back to the eighties, but it was not until the beginning of the new century, with the introduction of high accuracy, low cost desktop 3D printers, that layer by layer manufacturing become widely spread for industrial and scientific purposes [34]. 3D printing allows for numerous advantages with respect to traditional soft lithography: it allows for fully 3D structures and assemblies, low throughput time, speed up productivity and lower production costs. 3D printing is extremely useful for low cost rapid prototyping and point-of-care manufacturing, since the time between CAD design and production is shorten to a minimum and more designs could be fabricated simultaneously. It should be noted that 3D printing is a fully automated process that doesn't required highly trained personnel, moreover the design flexibility of additive manufacturing is way superior with respect to soft lithography and PDMS molding [6]. The main barriers to the extensive use of 3D printing for microfluidics reside in the difficulty to obtain accurate sub millimeter channels and internal features, along with the scarcity of truly optically clear materials [35]. Nevertheless, researchers' interest for this technology applied to microfluidics rose exponentially as soon as a new generation of high accuracy, high resolution, low cost printers and materials hit the market about ten years ago. Currently, among the different technologies commercially available, Stereolithography (SLA) and Material Jetting (MJ) have been proven to show a high relevance for microfluidic devices production [35]. Both technologies offer small features (layers

up to $14\mu\text{m}$), high accuracy printing, providing at the same time good reproducibility, low printing costs and allowing to print complex, fully 3D structures.

2.1.1 Stereolithography

Stereolithography was the first 3D printing technology being invented [34]. It exploits thermoset photosensitive liquid resins which undergo hardening (photopolymerization) when exposed to ultraviolet light. The parts to be printed are sliced in layers of fixed thickness, each layer is then realized by means of a laser which, exploiting a series of mirrors, selectively cures a viscous resin to form the required geometry. After the process is completed a printing base moves upward and a new layer is solidified by the laser; the operation is repeated until all layers are manufactured [36]. SLA is interesting for microfluidics since it allows to manufacture parts with high dimensional accuracy, 3D complex architectures, internal features and intricate details. Moreover surfaces are generally smooth and many resins are available, even biocompatibles. The most common desktop machines, produced by FormLabs and 3D Systems, could print layers ranging from 25 to $100\mu\text{m}$. [37] [38] Dimensional accuracy is fixed around 0.5%. During tests conducted with a FormLab Form 1+ desktop printer available in the lab, it has been shown that internal features up to $500\mu\text{m}$ can be printed with very good accuracy and reproducibility. Slightly smaller internal channels, until $350\mu\text{m}$ could possibly be printed under perfect printing conditions (new tank, new resin, perfectly clear mirror and very good orientation of the parts to be printed), but reproducibility is a big issue. Industrial machines can overcome these problems, offering an accuracy of $45\mu\text{m}$, but they come at a much higher cost [38]. To obtain higher mechanical properties SLA printed parts need to be post cured

by means of UV light of an appropriate wavelength. Post processing, like sanding and acrylic coating, can be used to further improve the optical properties of clear stereolithography resins. Appropriate drainage should be implemented for intricate internal geometries, thus posing a limit to design flexibility for microfluidic applications. Supports and parts orientation need to be well evaluated before manufacturing to obtain the best printing result possible. It should be noted that parts tend to become yellowish if exposed to sunlight, an issue that should be considered for research applications where perfect optical clearness is required. SLA dimensional accuracy and capability to print sub millimeter features is mainly determined by the laser spot size and resin properties, improvements in both direction are expected in the future. It should be noted that a similar technology, two photon polymerization (2PP), permits to print features as small as 200 nm [39]. This manufacturing process is theoretically very similar to SLA, but implies the use of two lasers. The biggest limitations of this process should be found in the extremely high cost of the equipment, around a few hundred thousand dollars, and the limited building size, which is constrained to a cube of a few centimeters. These drawbacks limit the diffusion of 2PP mainly to a purely academic use.

2.1.2 Material Jetting

Material Jetting is an additive manufacturing technology which uses a series of small nozzles on a printhead to distribute very small droplets of an ultraviolet curable polymeric material on a surface. The process is intuitively similar to the one used by common desktop inkjet printers. The liquid droplets are cured as soon as they are dispensed in the requested position, thus producing a solid structure. The part is printed layer by layer as in SLA printing, but material

jetting allows to obtain higher dimensional accuracy, smaller layer thickness, higher smoothness, fine details and better reproducibility of very intricate internal architectures. Composite structures, made of more than one material, can be manufactured with this technology, as well as colored parts [40]. Multi-material structure could be useful for microfluidics to introduce components with different stiffness and elasticity allowing for precise fluid control and manipulation. Parts printed with both SLA and MJ have homogeneous thermomechanical properties, although in the latter case no post curing is required, due to the extreme small thickness of the printed layers. Material jetting 3D printers can print layers up to $14\mu\text{m}$, with a dimensional accuracy of a few tens of microns [41]. Many materials are available, even biocompatibles. The printer distributes a disposable support material to fill every gap and guarantee that internal features do not collapse during manufacturing. The use of such process allows to obtain very complex internal architectures and designs. MJ class embeds PolyJet and MultiJet printing technologies. The main difference between the two cited technologies is to be found in the support material used. PolyJet, a technology by the Israeli company Stratasys, implements a water jet removable support material, which is also soluble in a 5% sodium hydroxide solution, while MultiJet, a technology from 3D Systems, uses a heat removable paraffin wax as support material [42]. In both cases there is no need for the user to manually remove the supports, avoiding possible damages to small features due to post-processing. Drainage should be accurately designed to guarantee a complete remove of the support material when internal structures are present. When dealing with PolyJet printed components, it should be noted that very long and thin internal feature can require lot of hours inside a NaOH solution to completely remove the

support material. In some cases a complete removal could also be unfeasible, thus practically posing limitations on specific designs. Nevertheless, delicate features can be damaged by an high pressure water jet, suggesting NaOH soaking as the best solution when manufacturing microfluidic devices. An Objet 30 Prime PolyJet printer, available at UIC Makerspace, has been chosen in this research to produce white resin mixers. A Stratasys J750 has been used to obtain transparent pieces. Since clear resin was not available at the Makerspace, the devices have been ordered online, printed and received in just a couple of days. What has been done shows one of the main advantage of 3D printing, the possibility to sent CAD files to producers and quickly obtain the desired products in a few days.

2.2 Materials

In this section attention will be posed on the PolyJet materials selected for the manufacturing of the devices used in this research. Stratasys offers a variety of materials for its PolyJet printers, in particular it's worth to notice a biocompatible product (MED610) for medical prototyping, a high temperature resin and the Vero family, a category which includes a series of polymeric formulations with good mechanical properties. Among the Vero family a transparent material (VeroClear) is present, this permits to obtain transparent but not perfectly optically clear parts. Better finish can be obtained by manually post processing the parts by sanding and painting. VeroWhite (RGD837) has been chosen as the material used to manufacture the first prototypes used for this work. VerClear (RGD810) on the contrary has been selected for the final designs, in order to test a complete enclose structure observable with a microscope. Mechanical properties of both materials are listed in Table I [43].

TABLE I: THERMOMECHANICAL PROPERTIES RGD837 AND RGD810

	METRIC	UNITS
Tensile strength	50-65	MPa
Elongation at break	10-25	%
Elasticity modulus	2000-3000	MPa
Flexural strength	75-110	MPa
Flexural modulus	2200-3200	MPa
HDT, °C at 0.45 MPa	45-50	°C
HDT, °C at 1.82 MPa	45-50	°C
Izod notched impact	20-30	J/m
Glass transition temperature	52-54	°C
Rockwell hardness	73-76	Scale M

VeroWhite is a whitish material which can be used to manufacture highly accurate parts and prototypes incorporating even moving features. It offers a good mix between strength, stiffness and flexibility, moreover it is heat resistant. VeroClear offers the same thermomechanical properties [44], but it is also transparent, but not perfectly optically clear. In this project a layer of $150\mu\text{m}$ of VeroClear has been used as the base for the designed micromixers. The layer is thin enough to obtain very good microscope images of the flow pattern inside the fluidic channel.

The support material chosen is SUP706 soluble material, which can be removed by water jetting and successive immersion in a 1 to 5% NaOH solution. Generally the support material is based on "propylene, polyethylene, acrylic monomer and glycerin" [35]. For this thesis pieces have been soaked in a 5% caustic soda solution for 4h, successively parts are drained, cleaned with compressed air and immersed for half an hour in a IPA bath. Remarkable improvement

in post-processing time and accuracy have been noticed if the printed parts are processed with an ultrasonic cleaner. From what experienced, when a design requires the use of very small features, ultrasonic bath is the only solution that guarantees the complete removal of support residuals from closed channels. The described post-processing procedure has been developed with a trial and error methodology, starting from the producer guidelines for support removal. The cited procedure is suggested for all those cases in which small, microfluidic compatible features should be printed.

CHAPTER 3

MIXER DESIGN

Microfluidic mixers are generally subdivided in two classes, active and passive, according to how mixing is achieved. Active devices usually exploit external forces (acoustic waves, magnetic and electric fields, temperature gradients) to induce disturbances in the flow and subsequent mixing [1]. On the contrary, passive mixers adopt a particular channel architecture to generate an appropriate flow configuration which enhances diffusion by increasing contact area and contact time [7] between two or more fluids. To the first category belong acoustically driven devices which exploit the vibration of microbubbles trapped in sidewalls cavities [15], sharp tips based mixers [45] and magnetically driven systems [7]. Passive devices usually achieve mixing by splitting and successive recombination of the fluids [46], T-shaped [10] and Y-shaped channels [11], sharp corner structures [1] or cascaded splitting and recombination structures [2]. For the following research the acoustically driven active design has been chosen. A second version of the mixer exploiting passive-like elements is proposed and used for performance comparison.

3.1 Design features and technological limitations

Acoustically actuated mixers usually avail of cavities on the main microchannel sidewalls to trap bubbles upon fluid injection. As explained in details in section 1.1, the dimensions of these grooves influence bubble size and consequently the mixing performances. Generally cavities have dimensions of few tens or hundreds of micrometers [47]. Contrarily to the most

commonly diffused acoustofluidic devices, in which bubble trapping is obtained by close ended internal features [15] [47] [48], the main idea for the following project is to design a device having holes open to the atmosphere (Figure 4). The liquid-air interface excitation would lead to the development of a microstreaming pattern. 3D printing (PolyJet) is chosen as manufacturing technology.

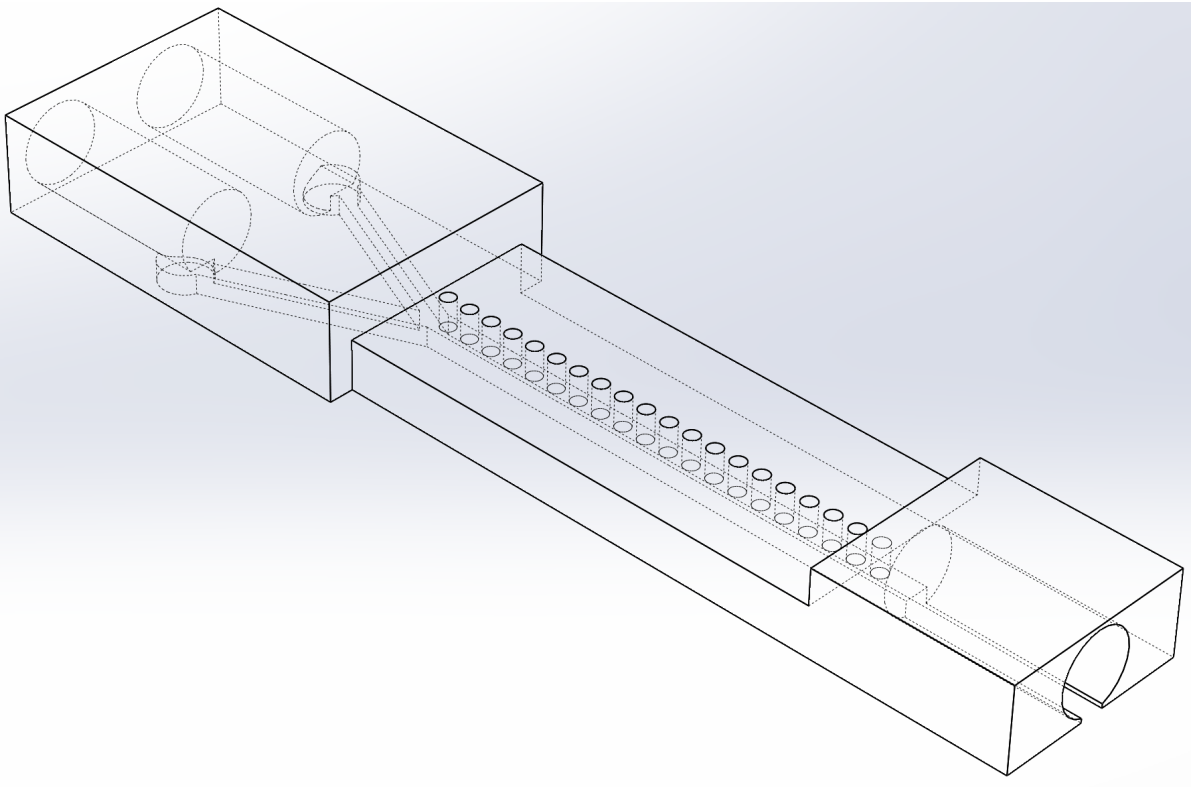


Figure 4: Design concept: active mixer incorporating throughout holes open to the atmosphere to allow for liquid-air interface development.

The proposed design allows to keep the liquid-air interface size constant even for prolonged applications, avoiding the possibility for the bubble to fade, as could happen trapping air in a close ended groove (PDMS is permeable to gases). The chosen design is easy, but usually it can not be fabricated in a single step: holes should be punched in PDMS to obtain a similar structure or pillars should be used during molding and successively removed. On the contrary, 3D printing fabricates the final device in a single manufacturing step, no handling of a green product is needed. The interest in this technology has faced an exponential rise in the last years, therefore it has been selected to test its benefits for microfluidic research. It is of great interest to show that basic microfluidic devices, like mixers, could be easily reproduced with 3D printing. Ideally, even personnel without a microfluidic background could select from an online library a mixer CAD file and proceed to printing, thus allowing point-of-care manufacturing. In addition, 3D printing is low cost, extremely fast (a few centimeters long device can be printed in less than half an hour) and allows for fast prototyping of many design ideas. Moreover, AM could allow to create intricate multi-material assemblies directly incorporating basic microfluidic blocks (mixers, pumps, gradient generators), thus eliminating the need for designing joints, jigs and fixtures, that are often prone to leakages and can introduce weak points in the structure.

3D printable models could be analysed by FEM softwares [6], allowing to simulate in advance the performances of elements under loads or thermal/pressure gradients. Models could be verified prior to manufacturing, discharging those designs who show failure during numerical simulations. This would allow for savings, since PDMS structures require experimental validation, a money and time consuming procedure.

The mixer design should meet strict constraints on dimensions and features. First, it is important to consider the need of sub millimeter structures to guarantee the compatibility for microfluidic applications. In particular selected dimensions should ensure the flow laminarity (low Raynolods number). The holes cut on the top face of the main channel should be big enough to show a fluid air interface, but the size should also allow for an appropriate level of surface tension to avoid leakages when fluids are pumped in the main channel. Along with functional limitations, technological issues should be considered too. PolyJet technology assures printable layers of $16\ \mu\text{m}$, while minimum external features dimension is set to $100\ \mu\text{m}$. The latter parameter is considered for supported walls and structures. Experiments suggest to print holes of at least $250\ \mu\text{m}$ in diameter. The main issues arising with holes are the post processing operations, since support material has to be removed with extreme accuracy and that could be sometimes hard to be done, even if the part is left for hours in a NaOH bath. Drainage should be properly taken into account, but in this case there is no need to develop particular support material removal solutions. Inlets and outlets have to be designed to interface the mixer to external equipment. In this case both interfaces have been modeled to fit standard 1/16" microfluidic tubing by a slight interference fit. Ideally, it would be possible to introduce in the design appropriate interfaces to obtain a modular architecture or connections for standard industrial fittings, like threads. To observe the flow pattern developed inside the device, the VeroWhite imposes the idealization of a design with one open side bonded to a slide glass. This concept introduces a few issues, since perfect hand bonding to a glass is extremely hard to be achieved, thus there is risk to have leakages and trap air sockets during operations. To solve

these problems and allow for printing a fully enclosed mixer, a clear but not perfectly optically transparent material (VeroClear) has been used for printing the final parts to be tested.

3.2 Design specifications

Three mixing devices have been designed and tested. An overview of each model and its main features is presented in the following sections, along with their history, from the first concept to the final product.

3.2.1 Basic design

A 3D model of the first structure is represented in Figure 4 and Figure 5. This is a purely active microfluidic mixer: the architecture is simple, consisting of two inlets for the fluids to be mixed, one outlet and a main channel with throughout holes open to the external environment on the top surface. Figure 5 (a) shows the CAD model of the last prototype version printed in VeroWhite resin and the final device used for testing (b - VeroClear). Engineering drawings can be found in Appendix A.

Figure 6 shows pictures of the actual device, notice the two inlets and one outlet (a) and the top holes (b). The picture present the final prototype model (VeroWhite), while the final device (in VeroClear) is very similar, but has fully enclosed channels.

The first mixer version exploited vertical inlets (Figure 7 a), that have been subsequently discharged for a planar structure. Nevertheless vertical inlets could be easily reintroduced if necessary. 27 holes (diameter $300\mu\text{m}$) are present on the top surface. Spacing between cavities is set to $500\mu\text{m}$. The main channel has a width of $500\mu\text{m}$, the two inlet branches have a width of $400\mu\text{m}$. Height of the channels is $400\mu\text{m}$. A second version of the structure used shorter

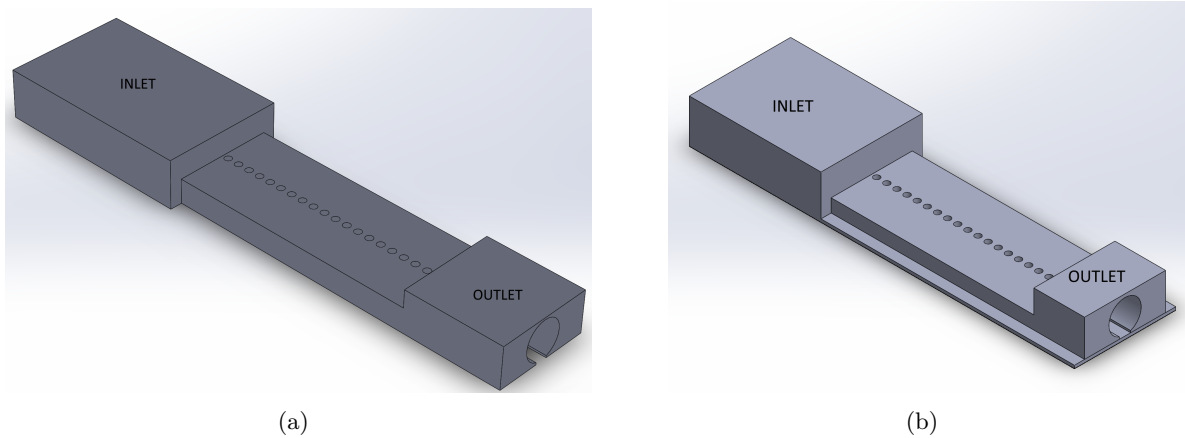
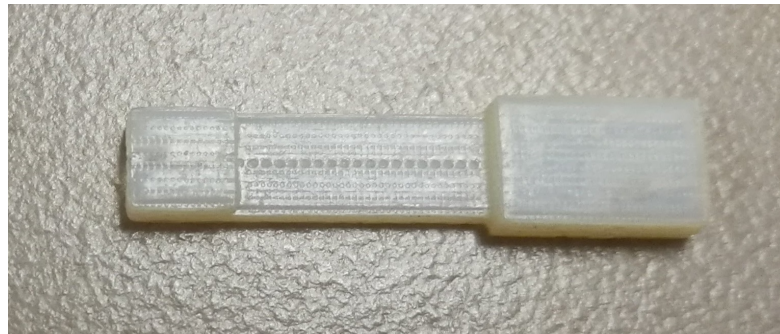


Figure 5: Mixer design concept, 3D CAD isometric view. Notice holes on top surface. (a) Prototype version. (b) Final design.

'Y' branches and a longer central body (Figure 7 b-c-d), the concept was changed to assess visually if the mixing was still working under slight geometrical changes. The latter design was soon abandoned, since the 27mm long main channel showed start of mixing at the end of the channel itself, probably due to the long fluids contact area. The third design, Figure 6, is shorter (19mm) and has 24 holes. This model defines the final prototype version for the basic mixer. The final mixer, as used for testing, is presented in Figure 8. VeroClear has been chosen as printing material, thus allowing for enclosed, transparent structures through which observe the flow. With respect to the prototype model, a $150\mu\text{m}$ thick base layer has been added and bonded to a slide glass. The choice for such a close device is twofold, first to avoid leakages from the glued layer, second to avoid the formation of air sockets during bonding. The main drawback of the used resin is the high reflection of fluorescent light occurring when a dye



(a)



(b)

Figure 6: Microfluidic mixer, basic design, VeroWhite. (a) Bottom view. (b) Top view.

is injected inside the channels, which introduces disturbances in the recorded images. With respect to the final prototype shown in Figure 6, the final design presents a shorter inlet block and a reduced central body height of $600\mu\text{m}$ (it was 1mm for the VeroWhite device); the choice has been made to minimize the material through which acoustic waves propagates. The Y-channels dimensions have been increased by $100\mu\text{m}$, to allow a better material drainage in the fully enclosed mixer. Inlets and outlet has been designed to accommodate standard microfluidic tubes by a slight interference fitting. If needed, more complex connectors, like threads or plugs,

could be implemented directly in the printed model. Thread printing accuracy should be assessed experimentally when small threads should be used. Interference fits are much easier to be designed, but leakages could arise if high flow rates are used. Inlet and outlet should be appropriately shaped according to the apparatus the mixer should be interfaced with.

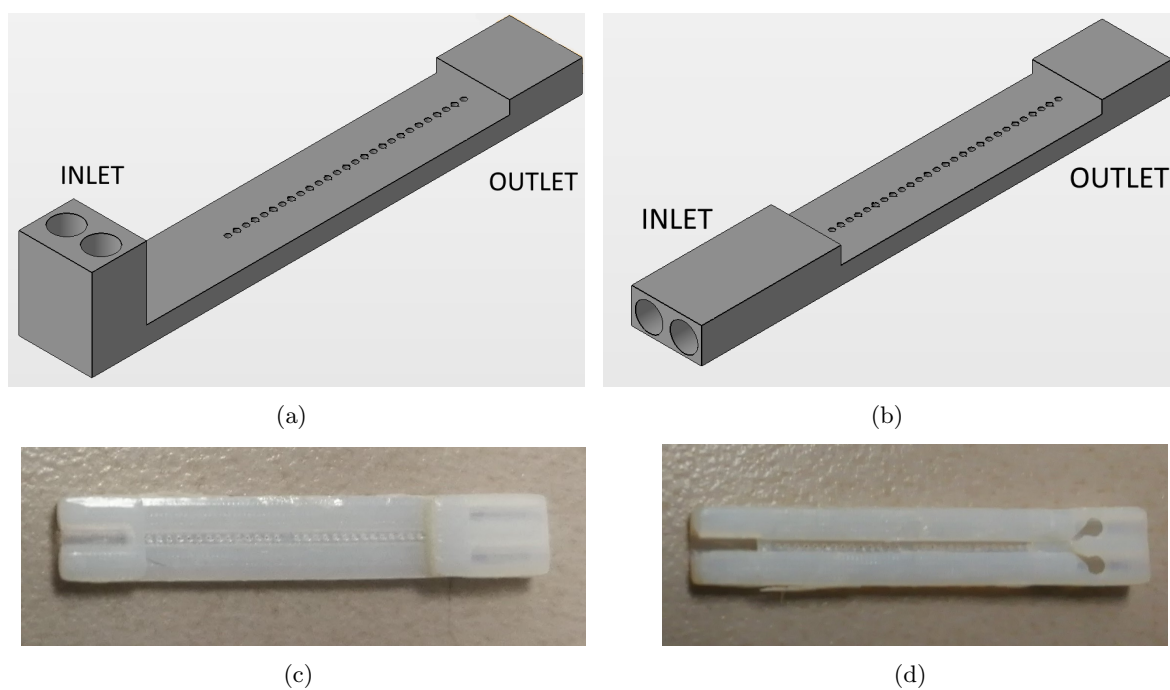
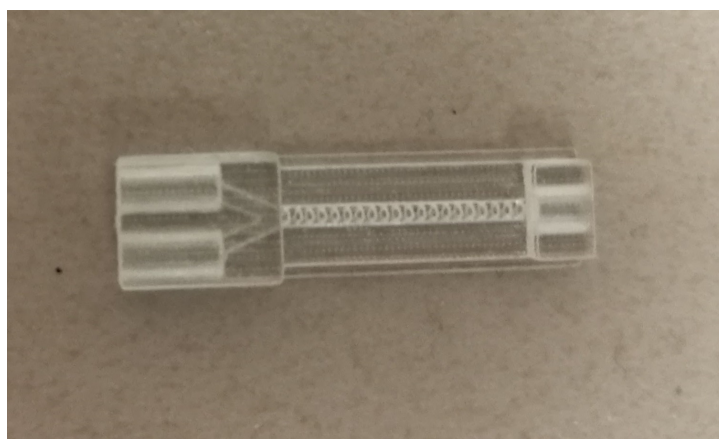


Figure 7: Microfluidic mixer, basic design. (a) CAD model first design, vertical inlets. (b) CAD model second design. (c) Second design, 3D printed, top side. (d) Second design, 3D printed, bottom side.



(a)



(b)

Figure 8: Microfluidic mixer, basic design, final version, clear resin. (a) Top view. (b) Bottom view.

3.2.2 Sidewalls hemispheres design

A second design has been ideated to further assess the printer capabilities. The new model, shown in Figure 9, introduces a passive-like element into the mixer architecture: hemispheres ($\varnothing 200\mu\text{m}$) are extruded on the main channel lateral walls and centered between two successive holes. The new feature should obstruct the fluid motion and disturb the laminar pattern.

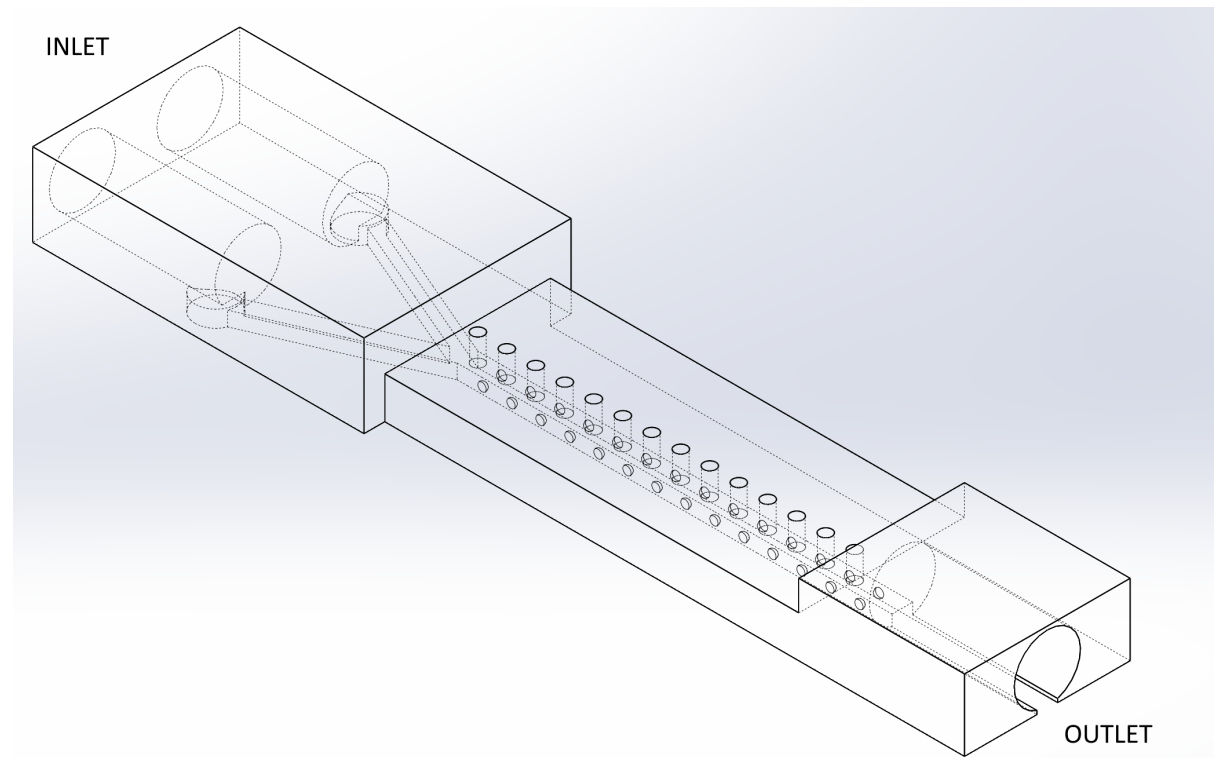


Figure 9: Sidewalls hemispheres design. Extruded $\varnothing 200\mu\text{m}$ hemispheres are centered between holes on the lateral walls of the main channel. First prototype CAD design.

Ideally, hemispheres are meant to enhance mixing; they should reduce the flow area, thus diminishing the available mixing volume when a time dependent flow disturbance is induced by means of an acoustic energy source. In this configuration the mixer has less holes (14) with respect to the basic design, spaced by $700\mu\text{m}$. The idea is to verify if it is possible to distinguish microstreaming and cross section reduction effects. Unfortunately, tests haven't displayed a clear distinction between the two phenomena, thus the distance between hole centers have been restored to $500\mu\text{m}$, as in the basic design presented in section 3.2.1.

Figure 10 shows a detailed bottom view of the main microchannel (3D CAD model). Notice the position of the the extruded sidewalls hemispheres inside the channel (here in black for a better graphical representation). Engineering drawings are available in Appendix B.

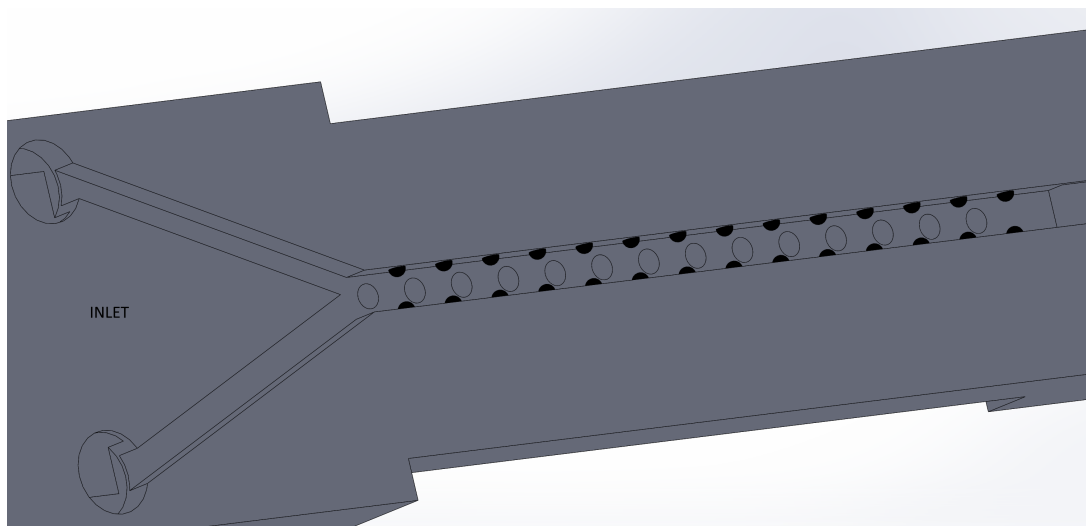


Figure 10: 3D CAD bottom view (prototype version) for the sidewalls hemispheres design. Notice hemispheres (in black) position on lateral walls.

A detailed microscope (Nikon Inverted Fluorescent Microscope Eclipse Ti-S/L, 4x magnification, bright field) view of a microchannel printed with VeroWhite resin is presented in Figure 11. The image has been chosen due to its significance: it shows the possible printing defects that can arise with PolyJet technology and the effect of short exposure time to a chemical bath. Notice how the top row of hemispheres are printed with poor dimensional accuracy and holes are still filled by support resin. Ideally all the black circular pattern should be dissolved. The latter problem can be addressed with a longer NaOH bath. The image shows is always good practice to check the parts at microscope before use. On average, printing a batch of five devices, at least one presents some kind of defects. Nevertheless if the degree of deviation from the original 3D model is low, mixing can still be observed, but mixing performances could vary. More details regarding the influence of printing accuracy on mixer performance are presented in section 4.3.

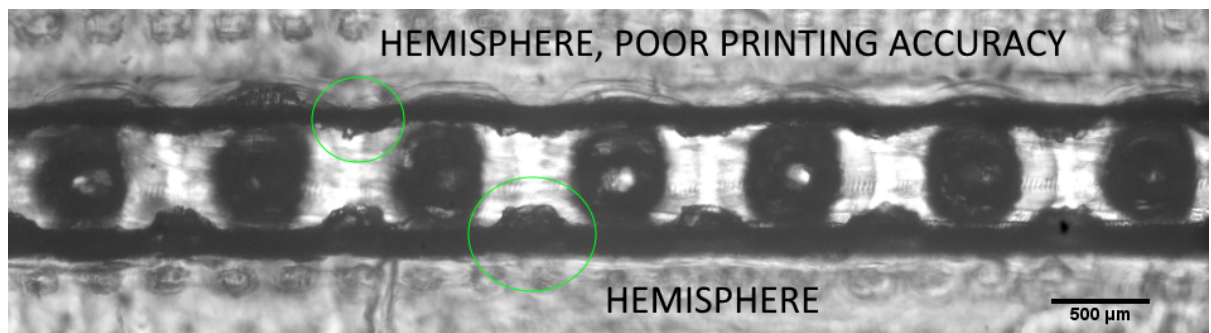


Figure 11: Microscope image of 3D printed micromixer, VeroWhite resin. Notice defects in hemisphere printing on the top wall and support resin still filled in holes (black material inside circular structures).

Figure 12 illustrates how holes look like after a complete support material removal. Notice a certain degree of deviation from the circular shape. Focus is set on the lateral hemispheres, consider the good shape of the feature in both rows, especially on the top one. With respect to Figure 11 the hemispheres have been printed with much more accuracy. The image also shows the final version of the sidewalls hemispheres design: distance between hole centers has been decreased to $500\mu\text{m}$, while the height of the central body has been reduced to $600\mu\text{m}$, to match the features size used for the basic mixer. As previously anticipated, a $150\mu\text{m}$ base has been added to enclose the main channel. The central microchannel width has been increased of $50\mu\text{m}$ to improve drainage of the closed system.

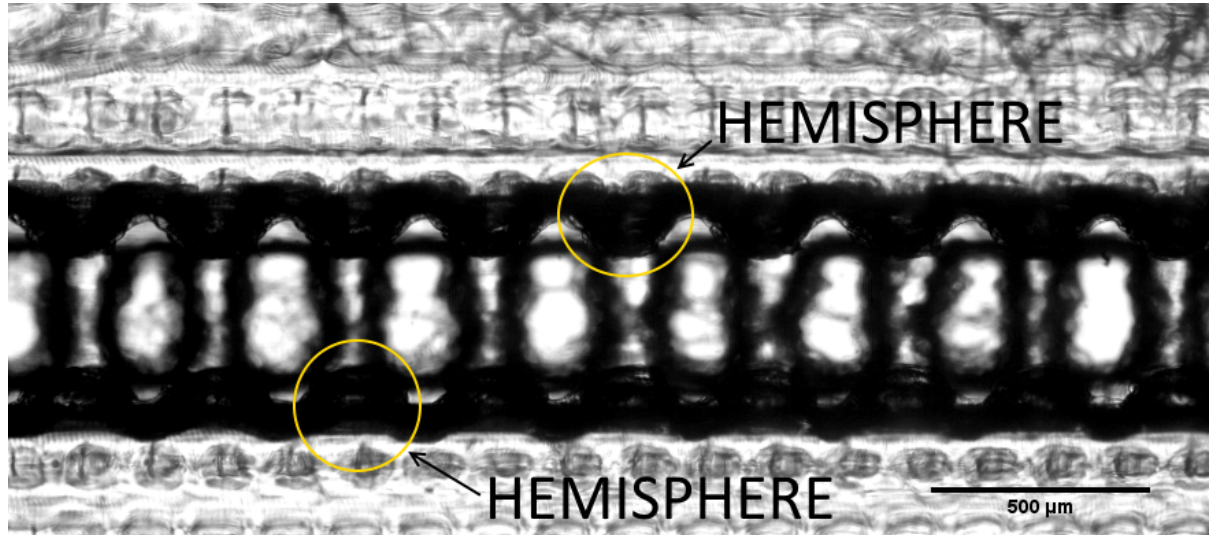
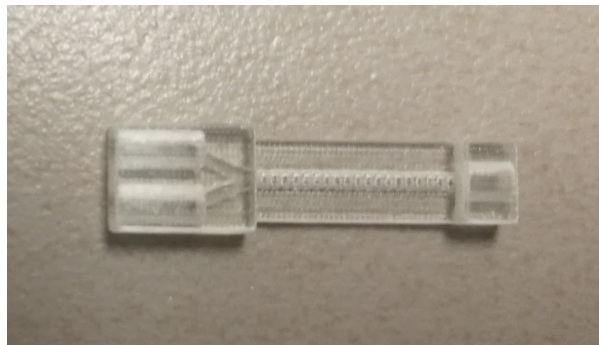
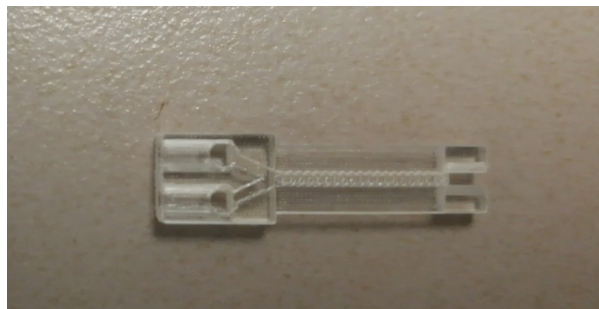


Figure 12: Hemispherical design, clear resin, 4x microscope view of the internal channel.

Images of the actual 3D printed mixers could be found in Figure 13. Sidewalls peaks are hardly visible, however notice the irregular profile in figure (b) which is actually due to this feature.



(a)



(b)

Figure 13: Microfluidic mixer, sidewalls hemispheres design, final version, clear resin. (a) Top view. (b) Bottom view.

3.2.3 Lateral channels design

For the last design concept, the basic design has been modified adding lateral channels on both sidewalls. The idea is to enhance mixing performances increasing the total liquid-air interface area. The conceptual design of this micromixer is shown in Figure 14. Engineering drawings can be found in Appendix C.

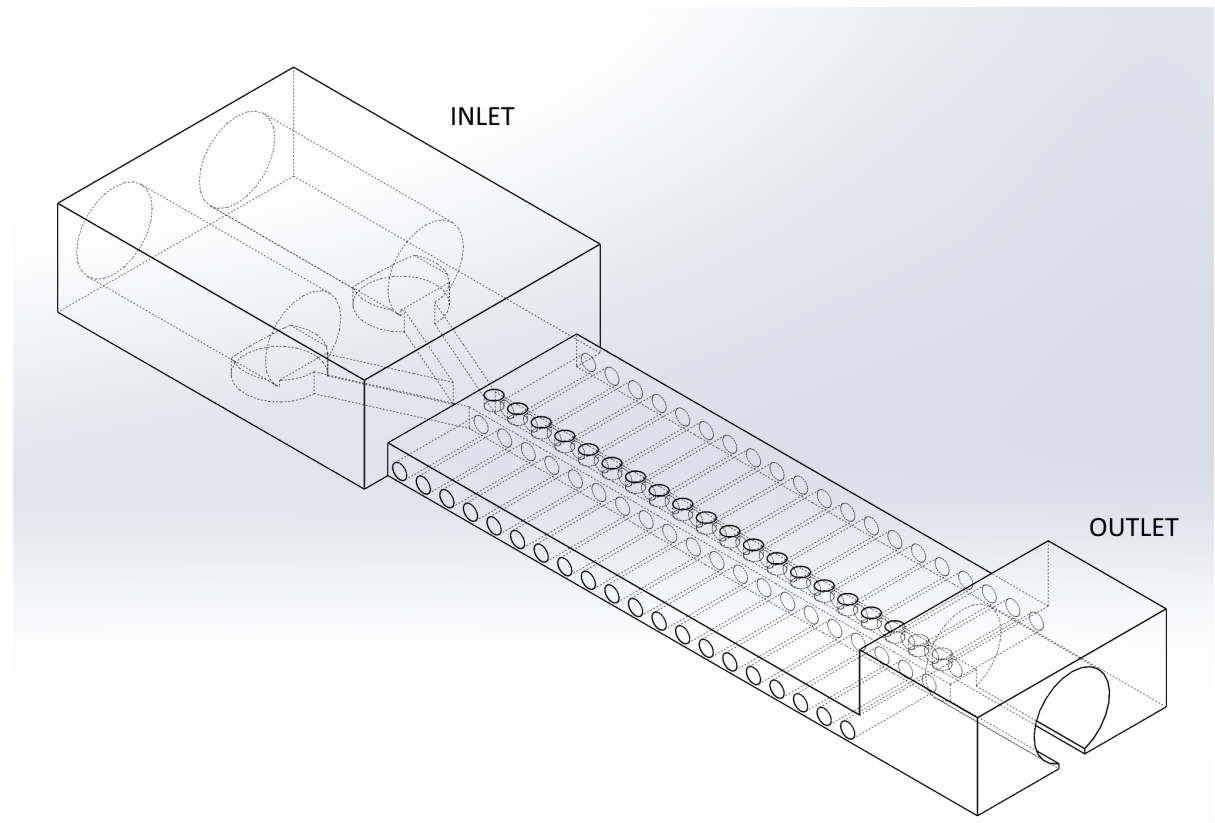
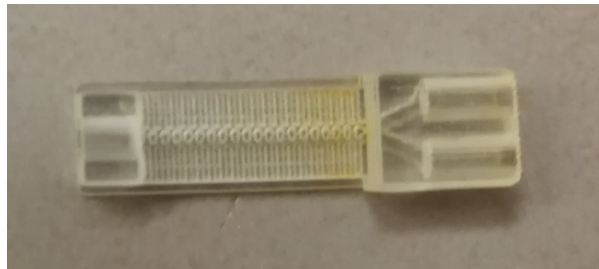


Figure 14: Design concept for an active mixer derived from the basic design. Channels are cut on both sides of the main microchannel.

Mixer geometry and dimensions are the same as used in the basic design presented in section 3.2.1. Circular channels with a $300\ \mu\text{m}$ wide diameter have been added on both sides of the main channel. The latter is $50\ \mu\text{m}$ wider, to enhance drainage. Conceptually, mixing enhancement should be achieved by increasing the number of cavities and thus the total liquid-air interface area, but concerns on manufacturability should be considered. Theoretically, the chosen printer has the resolution needed to print lateral channels of the selected dimensions, nevertheless support removal could be an issue, since the channels are narrow and long (1.75mm). The mixer, as printed in VeroClear resin, is shown in Figure 15.



(a)



(b)

Figure 15: Microfluidic mixer, sidewalls channels, VeroClear. (a) Top view. (b) Bottom view.

A detailed microscope view of the printed mixer is shown in Figure 16. Lateral channels are free of support, nevertheless this result is achieved with a long chemical bath (up to 12h) exposure combined with ultrasonic cleaning. Notice however that this procedure has damaged the top holes without fully emptying the lateral channels. In fact, it is easily noticeable that these channels have a diameter smaller than $300\mu\text{m}$; analysis by ImageJ shows that on average the lateral channels are about $130\mu\text{m}$ wide.

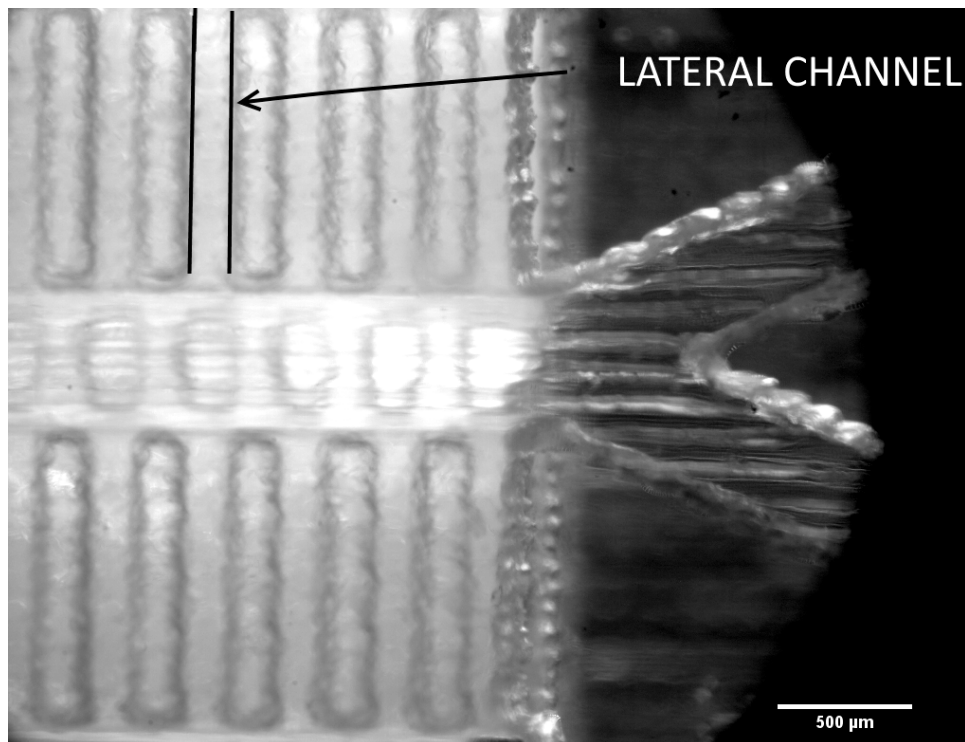


Figure 16: Microfluidic mixer, sidewall channels, VeroClear. (a) Top view. (b) Bottom view.

3.2.4 Design considerations

This brief section is meant to give a few design guidelines that should be followed to obtain good printing results with a PolyJet printer. Proposed dimensions and suggestion are based on the experience developed printing the various pieces presented in the previous subsections.

External supported features, like mixer walls and base, could be printed with a lower thickness as small as $150\mu\text{m}$, nevertheless the pieces are fragile and should be handled with care. During testing, the machine was able to print a base of $70\mu\text{m}$, nevertheless it was so small that it was destroyed during post-processing. Closed channels should be at least $300\mu\text{m}$ high and wide, but drainage could be difficult if extruded features are present inside the channels, in this case it is suggested to have at least one dimension higher than $500\mu\text{m}$. Throughout hole diameter should be at least $200\mu\text{m}$ (Figure 17) for cavities with a depth of a few hundreds μm , otherwise a diameter bigger than $300\mu\text{m}$ is suggested. Consider that deeper the channel is, wider should be the diameter.

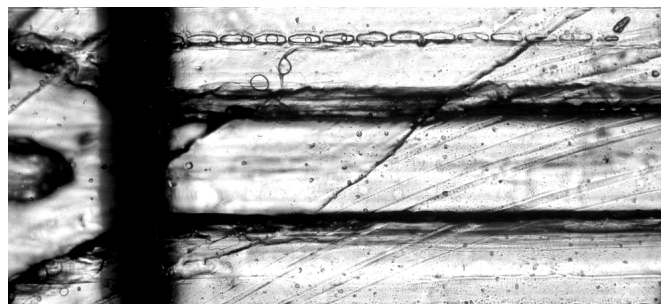


Figure 17: 3D printed channel, in the original design a series of top holes with $150\mu\text{m}$ wide diameter were present, but the machine was not able to reproduce the feature.

CHAPTER 4

RESULTS AND DISCUSSIONS

The following sections present the experimental tests conducted on the 3D printed mixers. After a brief introduction on the experimental setup and equipment used, the attention will be focused on data acquisition, analysis methodology and results discussion.

4.1 Experimental setup

Prototypes have been manufactured with a Stratasys Object 30 Prime 3D printer, using a white polymeric resin. Parts for testing have been printed with a Stratasys J750 printer, since clear resin was not available at the facility where the Objet was installed. It took one hour and a half to fabricate 30 pieces, subsequently parts are immersed for 4 hours in a 5% NaOH bath. Compressed air is used to remove impurities, eventually parts are soaked for half an hour into IPA. An ultrasonic bath is usually required for completely remove support material in closed channels. After a visual check with a microscope, devices are bonded (cyanoacrylate-based superglue) to a slide glass. Parts still showing support material residuals stuck into channels are soaked again in the chemical bath.

Inlets have been connected by standard 1/16" microfluidic tubes (Fluigent FEP) to a Chemyx Fusion 100 syringe pump [49]. A Nikon inverted fluorescent Eclipse Ti-S/L microscope [50] is connected to a Phantom Miro camera for image detection and recording (24fps). Videos are saved as .tif files and images are analyzed by ImageJ and MatLab. Fluorescein sodium salt

dye and fluorescent beads (Fluoro-Max green $4.8\mu\text{m}$) are used for flow detection by means of a blue light from a Nikon fluorescent filter cube. Liquid air interface is set in oscillation activating an ultrasonic piezoelectric transducer [51] actuated by a Rigol DG1022U function generator [52], connected to a Tegam model 2350 amplifier [53]. Figure 18 and Figure 19 show the experimental setup arranged for the experiments.

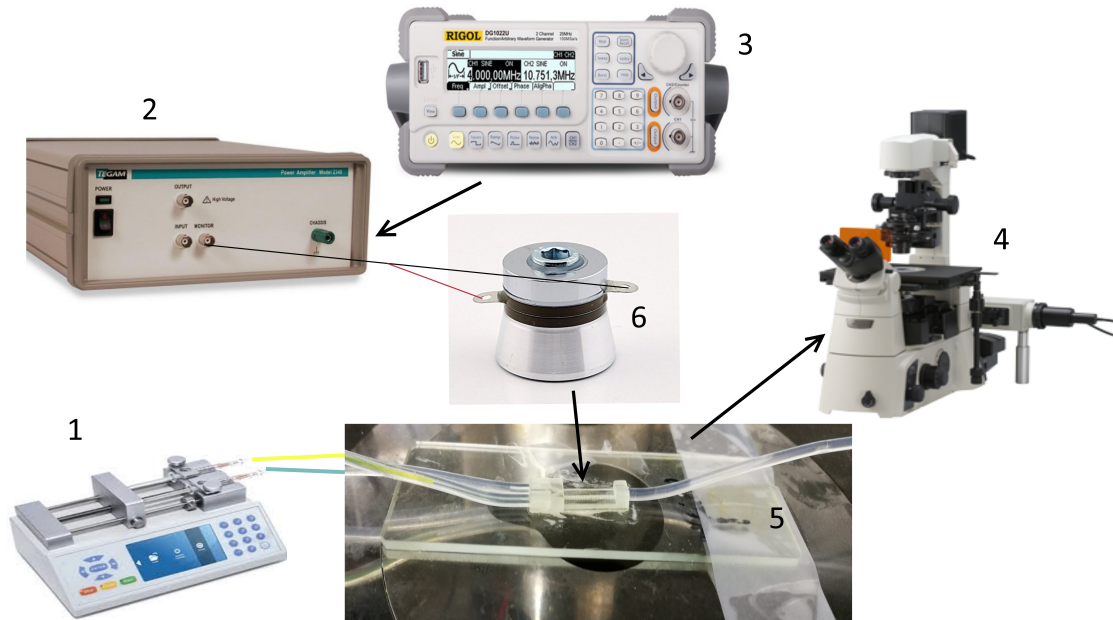


Figure 18: Experimental setup, schematic view. 1- Syringe pump. 2- Amplifier. 3- Function generator. 4- Microscope. 5- Piezoelectric transducer. 6- Mixer.

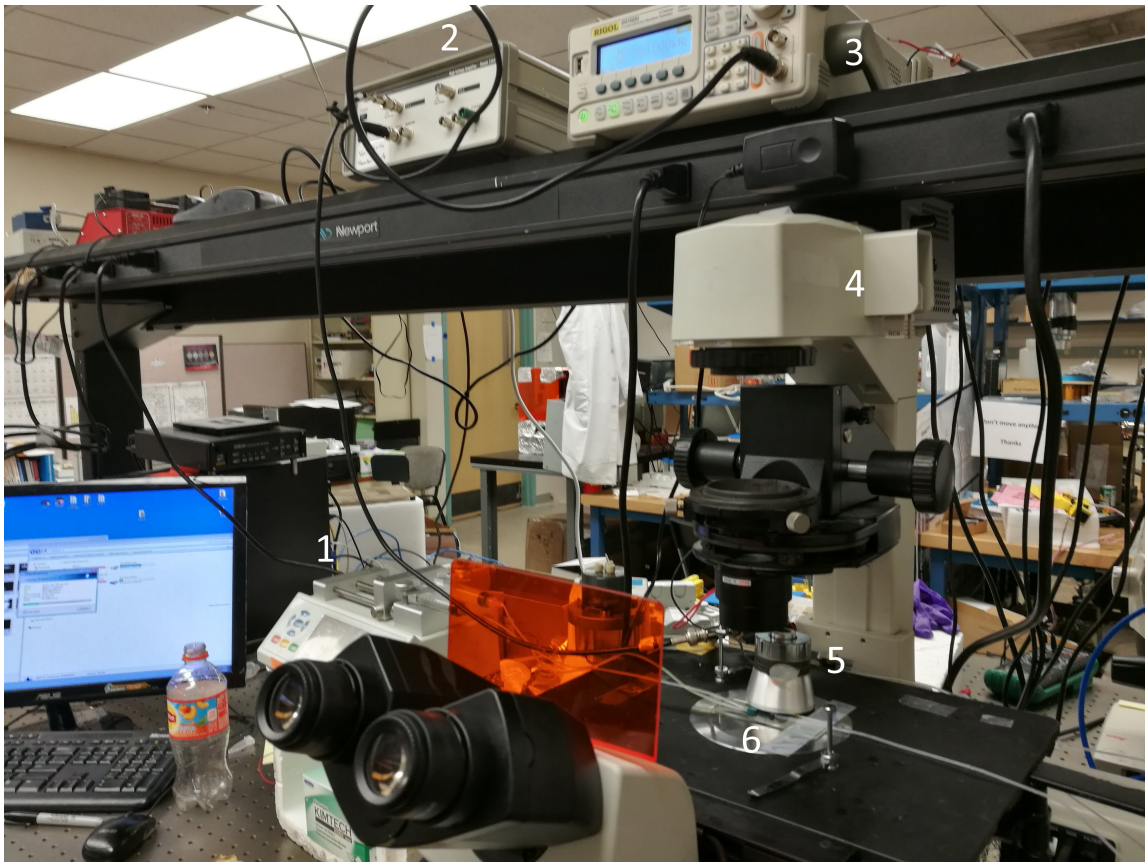


Figure 19: Experimental setup, lab equipment. 1- Syringe pump. 2- Amplifier. 3- Function generator. 4- Microscope. 5- Piezoelectric transducer. 6- Mixer.

Notice the syringe pump (1), connected by standard tubes to the microfluidic mixer (6), placed on the microscope (4). A function generator (3) is connected to a voltage amplifier (2), which drives a piezoelectric transducer (5) posed in proximity of the mixer. A camera plugged to the microscope (here not shown) records videos that are stored on a computer.

4.2 Laminar flow and microstreaming

To detect the mixing performances of the designed microfluidic devices, it is necessary to inject at the inlets two different fluids and visually guarantee the flow laminarity prior to set the liquid air interface in oscillation. Visual assessment of the phenomenon is performed using distilled water and a dye, fluoresceine. Laminar flow conditions occurs when the fluid flows in parallel layers. From a theoretical point of view, laminar flow is observed at low Reynolds numbers, a dimensionless parameter which express the ratio between inertial and viscous forces. The expression for Reynolds number is reported in Equation 4.1 .

$$Re = \frac{\rho u L}{\mu} \quad (4.1)$$

- Re Reynolds number;
- ρ fluid density (kg/m^3);
- u fluid velocity (m/s);
- L characteristic length (m)
- μ fluid dynamic viscosity (Pa.s).

For a rectangular channel, the characteristic length is calculated as the ratio between four times the cross sectional area of the channel and the the channel wetted perimeter, defined as the total perimeter of the cross section that is in contact with the fluid [54]. For the chosen cross channel dimensions, the parameter varies from 0.111 for $3\mu\text{L}/\text{min}$ flow rate to 0.74 when syringe pump is set to work at $20\mu\text{L}/\text{min}$. Being the Reynolds number much smaller than

unity, the data show, theoretically, the laminarity of the flow. Experimental tests confirm the hypothesis, as show in Figure 20 and Figure 21.

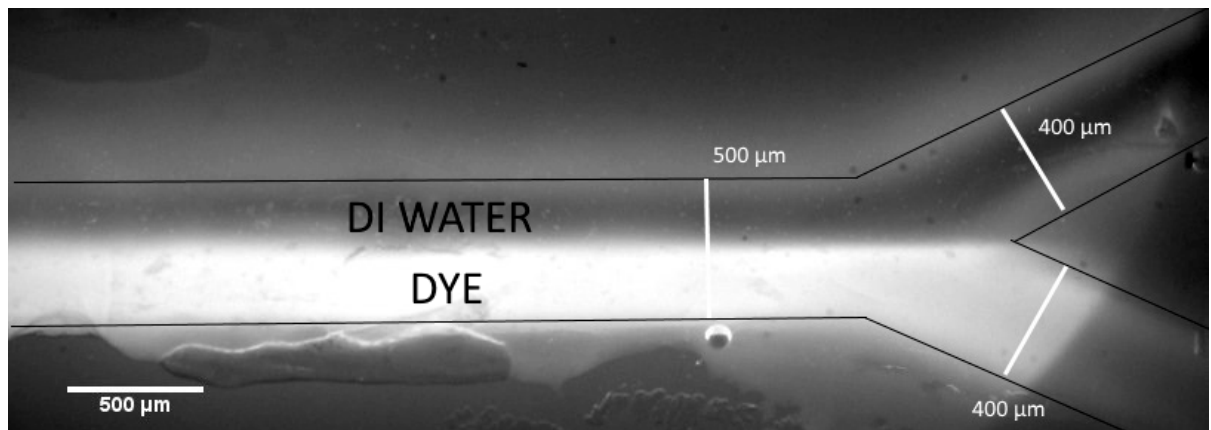


Figure 20: Laminar flow patter, basic mixer design, white resin prototype. 4x magnification.

Before evaluating the mixing performances of the devices, $4.8\mu\text{m}$ fluorescent particles are employed to observe the microstreaming pattern induced by fluctuations in the liquid-air interfaces at the top surface holes. A syringe pump is used to contemporary inject fluid from two 10ml syringes (DI water + beads and only distilled water) at a costant flow rate. It is useful to remark again that disturbances in the flow are induced by the acoustic coupling which develops between sound waves and liquid-air membranes upon activation of a piezoelettric transducer. The interface oscillation is responsible for the development of pressure and velocity instability patterns rapidly affecting the surrounding fluid, producing the so called microstreaming

phenomenon. Direct physical consequence of microstreaming is a bulk fluid flow that breaks the laminarity pattern [15] [21]. Exploiting cavitation microstreaming it is possible to design devices for rapid fluid mixing [55].

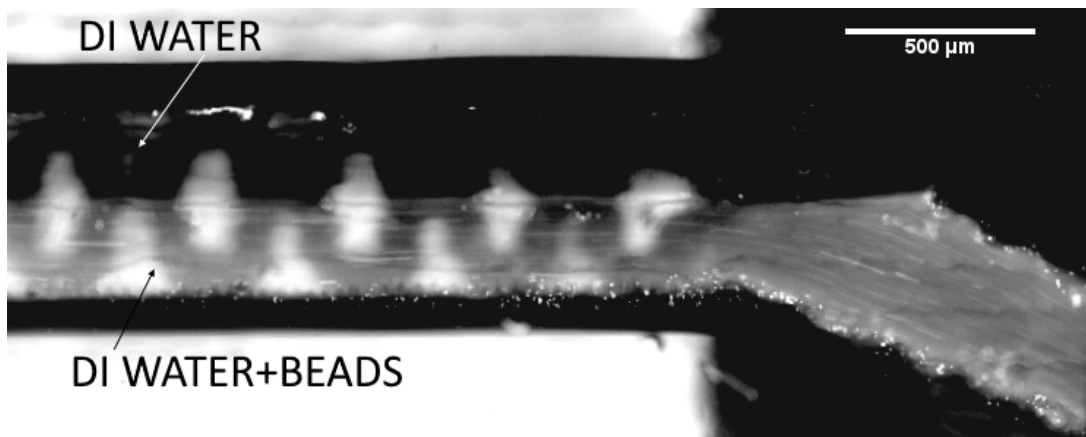
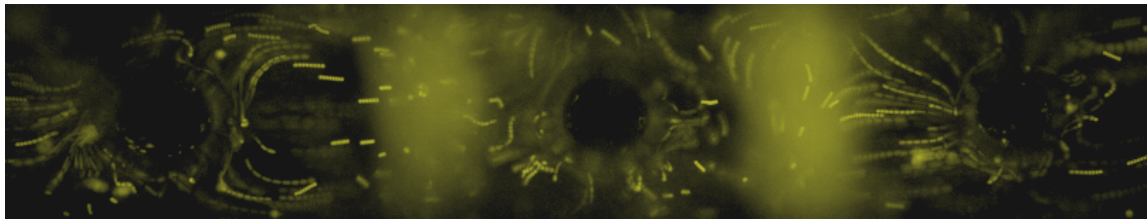


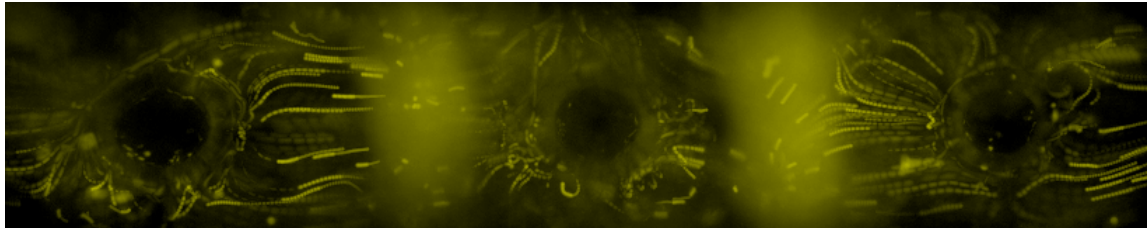
Figure 21: Laminar flow patter, basic design, clear resin. $4.8\mu\text{m}$ fluorescent beads.

Images of the flow disturbances induced around three adjacent holes for the basic design are found in Figure 22. The pictures are obtained by super imposing 5 recorded frames (a), 10 frames (b) and 200 frames (c) by means of ImageJ Z projecting function. $4.8\mu\text{m}$ beads were used, notice the trajectory deflecting as particles approach the cavities with bubbles. Compared to what shown in Figure 21, in which beads+DI water and DI water were injected by means of a syringe pump to obtain the laminar flow profile, in this case a mixture of water and beads is injected in the channel and the syringe is stopped. Therefore, the trajectories

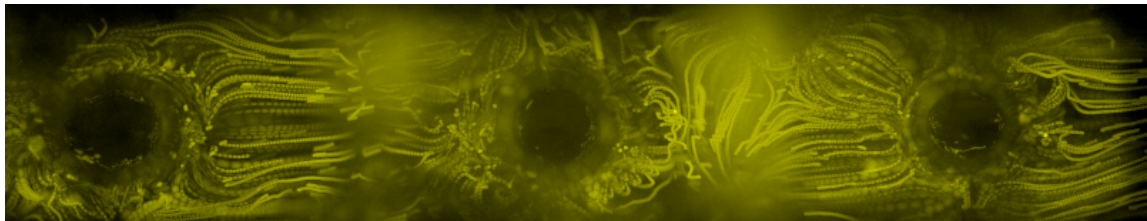
here shown are produced uniquely by microstreaming. Consider that this kind of images are hardly reproducible with a clear resin, due to the high amount of noise introduced by reflected fluorescent light coming from the excitation of beads. For this reason, the following figures are recorded using the prototype version of the mixer made with white resin.



(a)



(b)



(c)

Figure 22: Microstreaming patterns around three consecutive holes, basic mixer design. 10x enlargement. (a) 5 frames composition. (b) 10 frames composition. (c) 200 frames composition.

A 20x enlargement of beads trajectories around two consecutive holes is presented in Figure 23. The image is a composition of 50 subsequent frames. Blurriness in the first hole was probably due to some beads stuck on the glass (bottom layer) which introduced noise in the recording process.

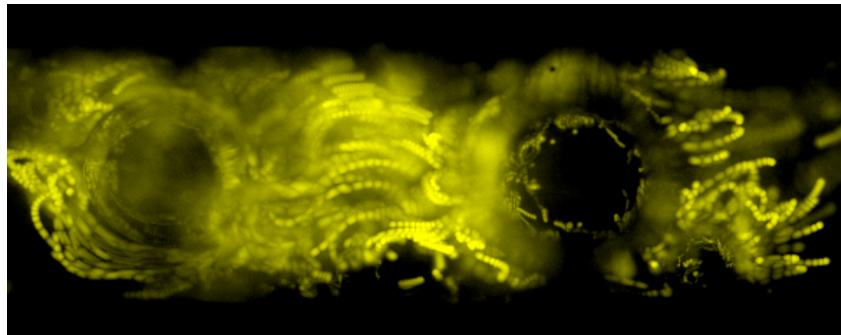


Figure 23: Microstreaming patterns, basic design, 20x magnification.

Figure 24 visually shows the induced microstreaming effects in the design embedding sidewall hemispheres. Position of the extruded features is indicated on the image (composition of 100 fps), notice that, as already discussed, hemispheres are slightly different one another. Consider also the dimension of the left bubble, which is objectively smaller in respect to the second one. The issue is probably imputable to some support material residuals into the hole or a partial development of the bubble itself during fluid injection. Syringe pump was turned off, therefore flow patterns are to be ascribed to cavitation microstreaming only. Notice in Figure 24 that the

two bubbles produce different effects on the bulk flow, which can be ascribed to discrepancy in radii dimensions. The image suggest the frequency in use is closer to the resonant frequency of the left bubble.

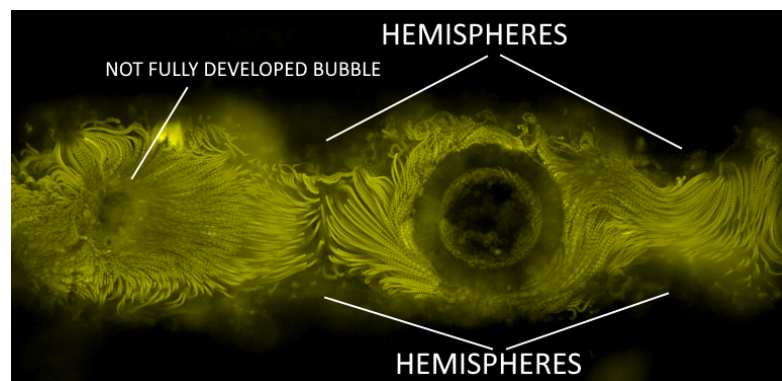
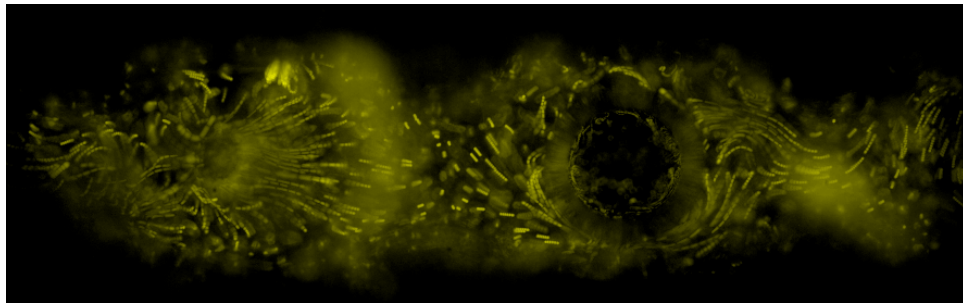


Figure 24: Microstreaming patterns, design with hemispherical features on sidewalls. Notice incompletely developed bubble on the left and the hemispheres. 10x magnification.

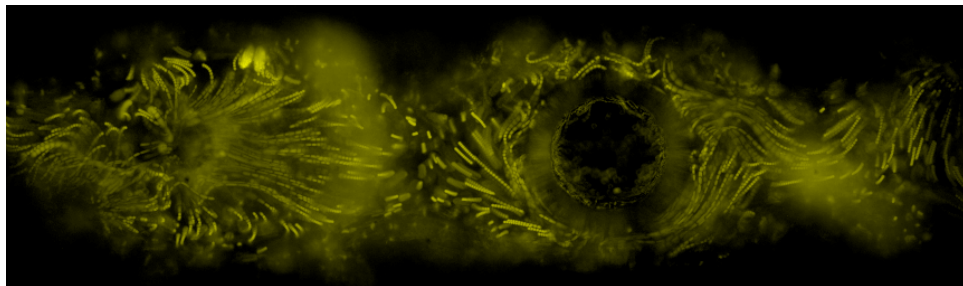
Figure 25 shows an enlargement (10x magnification) of beads trajectories for the hemispheres design. Images are obtained superimposing 5 (a) and 10 (b) subsequent layers by ImageJ.

The visual results presented in this section guarantee all the theoretical hypothesis made during the design phase. Channels dimensions have been correctly selected and superficial roughness is small enough to avoid the development of visually noticeable disturbances in the flow. Holes are small enough to prevent liquid leakages and can be use to develop liquid-air interfaces. The membranes can be set in vibration by means of acoustic waves, the developed

microstreaming is able to induce disturbances in the surrounding bulk fluid. At this point, the next logic step is to directly evaluate the mixing performance and reliability of the designed microfluid devices. Notice that, as shown in Figure 24, some issues could arise in the liquid-air interface development. Until now it has been proposed only a visual and qualitative representation of the mixing phenomenon, detailed quantitative measurements of mixing performances should be investigated in the next section.



(a)



(b)

Figure 25: Microstreaming patterns around three consecutive holes, sidewall hemispheres design. 10x enlargement. (a) 5 frames composition. (b) 10 frames composition.

4.3 Mixing performance

The following section is ment to give a detailed overview on the mixing performances and releability of the printed microfluidic components. A quantitative analysis is carried out using MatLab and ImageJ. Short videos showing the flow conditions in the main channel as the piezoelectric transducer is turned on and off are recorded (24 fps). DI water and a DI water+fluorescein solution are injected at the two inlets by means of the syringe pump. Voltage and syringe pump flow rate are the parameters to be varied. Function generator is set to produce a square wave of a certain frequency, the frequency spectrum is swept manually to determine experimentally the working frequency range for a particular device. Slight discrepancy between mixers are to be ascribed to small differences in liquid-air interface size. Usually, mixing is gauged analyzing a series of frames recorded over a certain period of time, by means of an appropriate mathematical function. The function, called mixing index, returns a dimensionless parameter which is useful to describe the degree of mixing. The index is bassed on the measure of a standard deviation. Different formulations of the index have been proposed and used in the past [15] [56] [57], thus leading to some issues in comparing the work of different authors. In the following analysis the Relative Mixing Index (RMI) [57] will be used. As the name indicate, it has the advantage of being a relative parameter, slightly affected by initial conditions, light intensity and dye used [57]. The mathematical definition of RMI is found in Equation 4.2. The index compares the standard deviation of the pixel intensities across a given cross section at a certain time T with the standard deviation of the pixel intensities at the same cross section for

time T_0 , where T_0 represents the unmixed condition (laminar flow). The index ranges from 0 to 1, being 0 representation of the unmixed case and 1 denoting total homogeneous mixing.

$$RMI = 1 - \frac{\sigma}{\sigma_0} = 1 - \frac{\sqrt{\frac{1}{N} \sum_{i=1}^N (I_i - \langle I \rangle)^2}}{\sqrt{\frac{1}{N} \sum_{i=1}^N (I_{oi} - \langle I \rangle)^2}} \quad (4.2)$$

- *RMI* Relative Mixing Index;
- σ standard deviation local pixel intensities across a cross section;
- σ_0 standard deviation local pixel intensities across a cross section, unmixed case.
- N total number of pixel in a cross section;
- I_i local pixel intensity;
- I_{oi} local pixel intensity, unmixed condition;
- $\langle I \rangle$ average pixel intensity in a cross section;

The procedure to evaluate the RMI starts with a manual data collection by means of ImageJ. Videos are analyzed with the following procedure. The first frame showing the beginning of the mixing phenomenon is detected, the antecedent frame is considered as the unmixed state. A cross section representative of the channel is selected, twenty subsequent frames are measured, starting from the unmixed state. ImageJ returns automatically some values (Appendix E), like minimum and maximum pixel intensity in the selected cross section, average pixel intensity and standard deviation of intensity. The latter parameter is the one of interest for the evaluation of the RMI. Since data are recorded at 24 fps, twenty frames spawn around 833ms. The

ratio of the standard deviation between mixed and unmixed state is calculated as expressed in Equation 4.2 by means of a custom made MatLab script. A general version of the script is reported in Appendix D, the software is used to calculate the RMI and plot the obtained results. The drawback of the methodology here reported relies mainly in the difficulty to select the same exact cross section in different videos recorded at different time, a slight variation on the number and position of the selected pixels is always present. Moreover, unmixed condition could show slight intensity variations, since some dye residuals could remain stuck into the channel. The total introduced noise is small, it produces fluctuations in the results of around 8%, but it does not influence their trend.

4.4 Results

An analytic overview of the mixing performances of the designed devices is given in this section. All mixers are made with VeroClear transparent resin. All tests, except where expressly stated differently, are conducted at 41 kHz. Basic trends of the relative mixing index as function of the applied voltage or flow rate are first proposed. Subsequently, a short performance comparison between the different design is given.

4.4.1 Basic Design

Figure 26 indicates the cross section selected for calculating the mixing index for the basic design. Flow rate is kept constant at $20\mu\text{l}/\text{min}$, the amplitude of the generated square wave is swept in the range 20-5Vpp. Results are plotted in Figure 27. Notice, as first aspect, the growing trend of the mixing index as the elapsed time increases, a behaviour already reported in literature for micromixers [57].

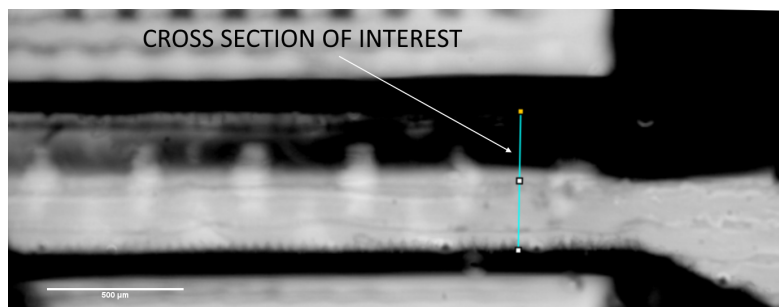


Figure 26: Section of interest, basic design, VeroClear resin.

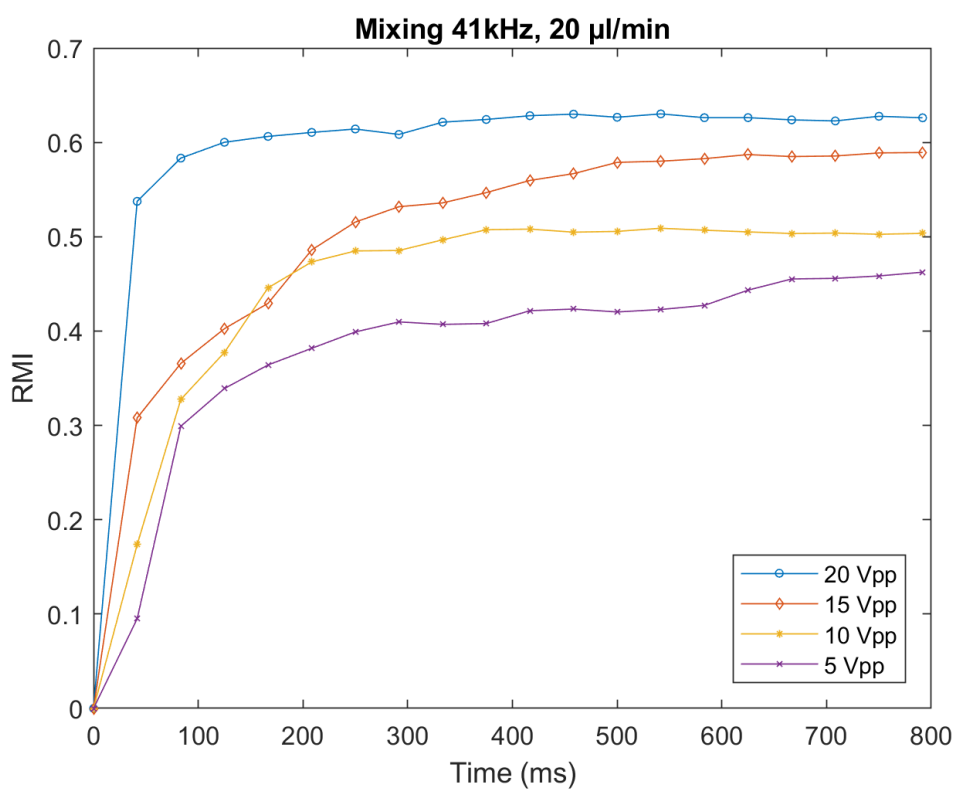


Figure 27: Mixing index at 47 kHz and 20 μl/min.

The effect of the peak to peak voltage is straightforward, higher voltages correspond to a higher power, according to the physical law that relates the electric power with the square of the applied voltage. In turn, a change in power corresponds to a variation in the amplitude of the wave produced by the piezo and a change in the oscillation amplitude of a bubble. A 5 peak to peak voltages leads to the lowest results in the range analyzed, experiments have shown that going to 1Vpp would lead to a very slow response of the system. Notice that after around 500ms the mixing index for most voltages tends to converge. The difference in applied voltage is particularly influencing the behavior of the mixer in the first 100ms. The response of the device, here expressed by curve steepness, decreases with decreasing applied voltage, at 20Vpp it takes only 41ms (frame 2) to reach a mixing index about 0.54, while 5Vpp leads only to a RMI of 0.1. At 167ms (frame 5) the 10 Vpp curve shows a mixing index slightly higher than the RMI of curve 15Vpp, this discrepancy can be explained with the experimental nature of the used data. As remarked in section 4.3, small oscillations in the converging areas of the curves are inherent to the methodology used to collect and post-process the data, notice though that the averaged value of each curve shows a constant behavior.

A further section located between holes 3 and 4, as show in Figure 28, has been chosen to test the design capabilities as function of the flow rate produced by a syringe pump. In this case the relative mixing index is calculated keeping the voltage constant at 20V peak to peak, while the flow rate set by the syringe pump has been varied in the range 20-3 μ l/min. Results are reported in Figure 29. As for the previous experiment, the fluids used are DI water and fluorescein dye.

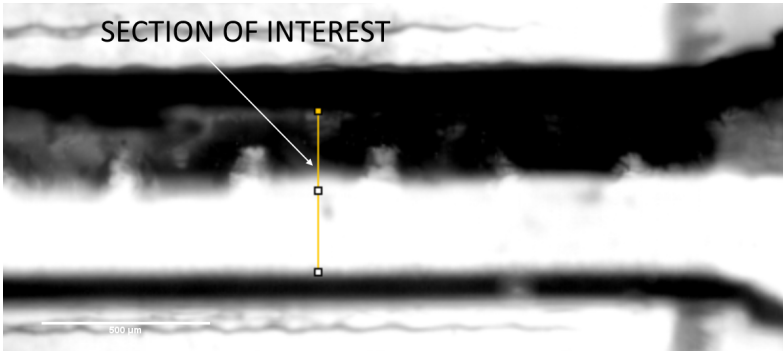


Figure 28: Cross section of interest, basic design, VeroClear resin.

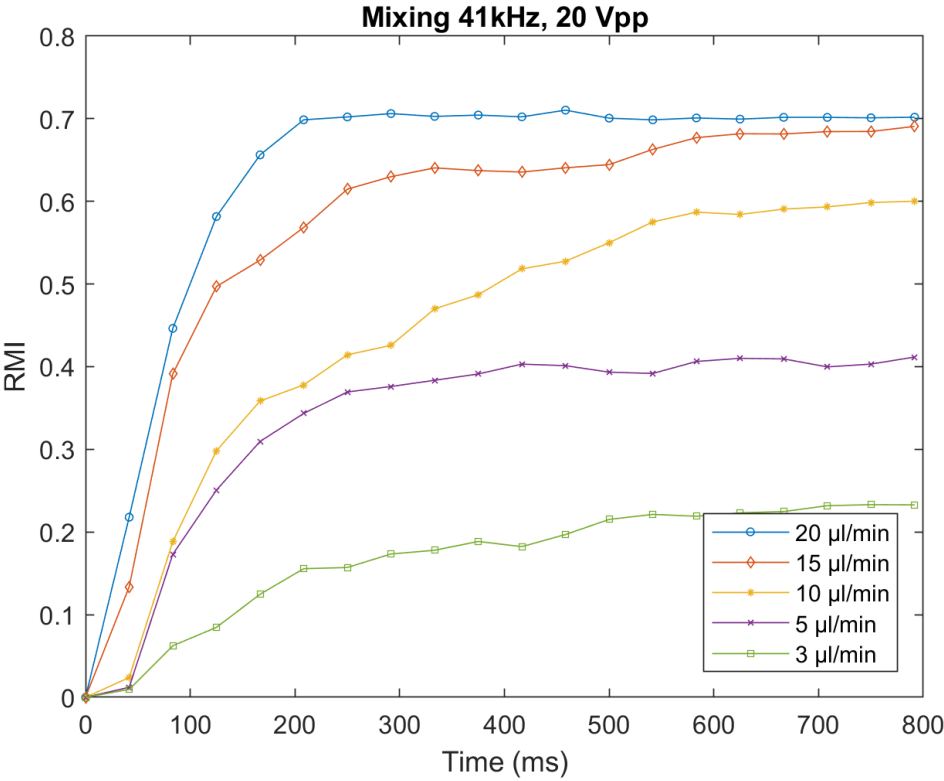


Figure 29: Mixing index at 47 kHz and 20Vpp.

Figure 29 clearly highlights the relation between flow rate and mixing index. As the flow rate increases, the gradient between the two species (DI water and dye) becomes stronger, thus improving the diffusion process. A very small flow rate, $3\mu\text{l}/\text{min}$, yields a very low RMI, thus this mixer is not suitable for such low flux values. Notice as both $20\mu\text{l}/\text{min}$ and $15\mu\text{l}/\text{min}$ tends to converge to the same RMI value after 600ms, which is the maximum mixing index such device could achieve. Consider also that in Figure 27 the maximum value of RMI is 0.6, while here is 16% higher. Explanation for this behavior should be found on the difference of cross section selected. In the latter case the effect is produced by 4 holes.

As indicated by the curves shown in Figure 31 and in accordance to what shown in Figure 29, the mixing index is influenced by the flow rate set by the syringe pump. The number of holes influence the mixing index, since pre-mixed fluid passes through consecutive areas of induced flow disturbance.

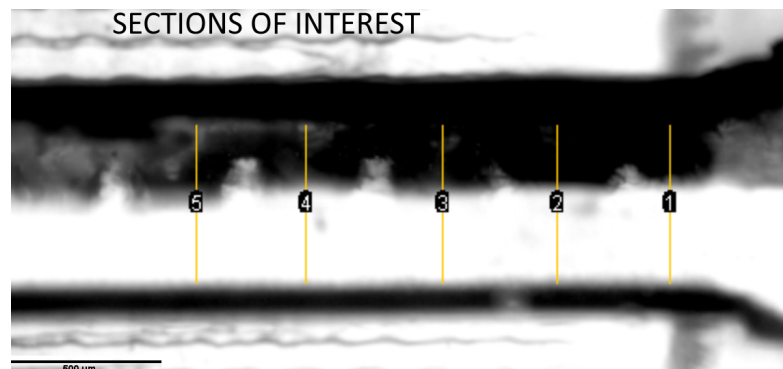


Figure 30: Sections of interest, case relating number of holes and RMI.

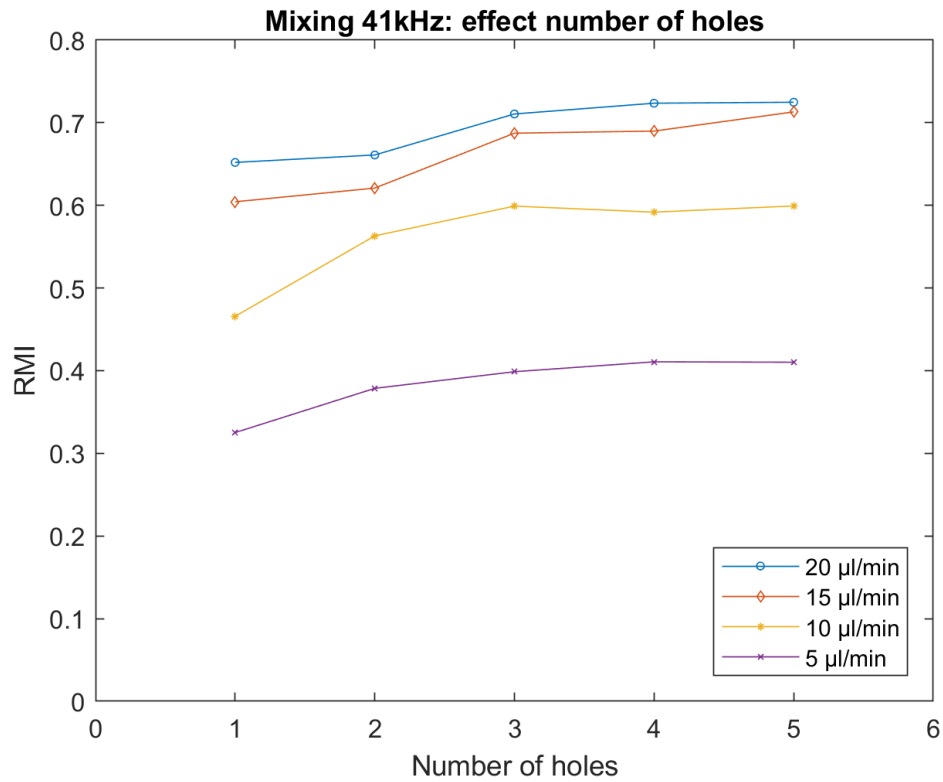


Figure 31: Relation between mixing index and number of holes at 450ms.

A good overview on the effect of holes on the relative mixing index is shown in the plot of Figure 31. Five different sections have been considered, as shown in Figure 30. Results indicate that model evaluation for 5 holes is a good choice, since the relative mixing index tends to converge already after 4 holes. The highest influence is detected shifting between hole 1 and 3.

Convergence of the mixing homogeneity is shown in the chart in Figure 32. Notice that it takes less than 400ms to reach a stable mixing index, thus allowing this mixer to be used

for all those application in which maximum mixing should be obtained quickly. The index is calculated in the section show in Figure 26.

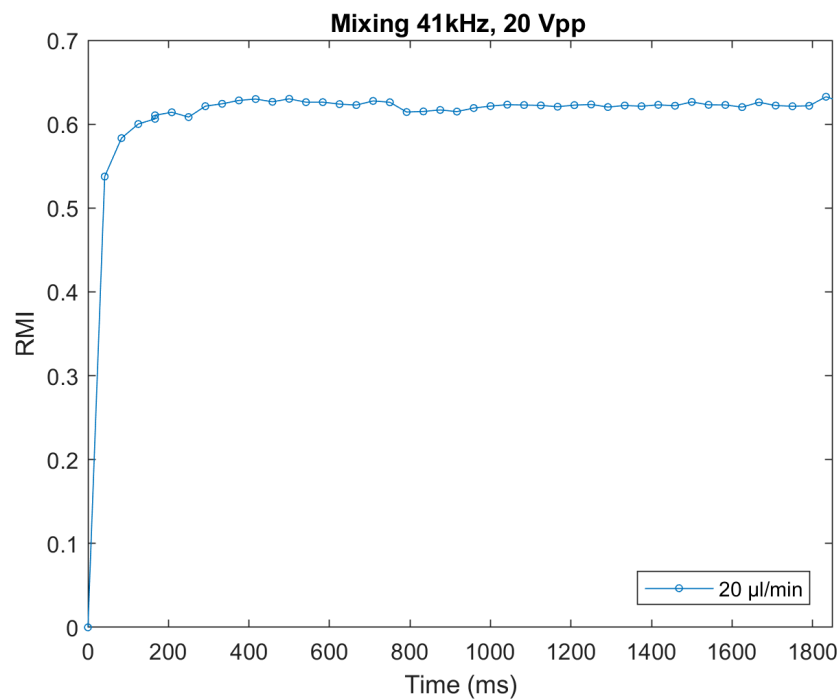


Figure 32: Convergence of RMI for basic mixer design.

The relative mixing index is an important indicator of the mixing efficiency of a certain microfluidic device. Nevertheless being its value calculated as a standard deviation weighted average of pixel intensities through a cross section, it doesn't give quantitative data on the mixing homogeneity across the width of a microchannel. Mixing homogeneity is thus analyzed

taking into account the normalized intensity of each pixel through a generic mixer cross section.

Results shown in Figure 33.

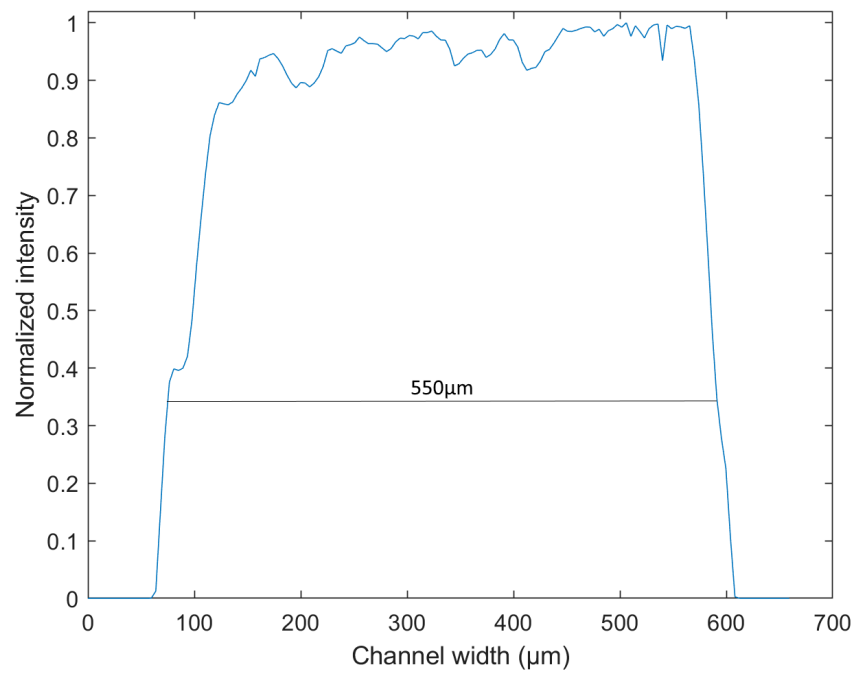


Figure 33: Mixing homogeneity through a generic cross section.

Normalized intensity is 1 when the mixer has produced perfect mixing, while is 0 in the unmixed state. According to the graph, mixing has a good homogeneity across a generic channel cross section. The error in homogeneity is 7.07 % (data have been post-processed to exclude outliers).

4.4.2 Sidewall hemispheres design

For the sidewalls hemispheres design, relative mixing index is calculated in a the narrow area of the channel, in position as much similar as possible to the one used in section 4.4.1. Figure 34 illustrate the section of interest used for the evaluation of RMI (Figure 35) as function of the applied peak to peak voltage, at constant flow rate. Notice that in this case lateral features are printed with a good accuracy, especially on the top side of the channel. Unfortunately, using the microscope, a choice on which level to focus on should be made, thus reducing the clearness of the picture. At the same time resin roughness and the high reflection due to the injected fluorescein, contribute to make the images a bit blurry. Nevertheless, ImageJ is able to accurately evaluate the difference in standard deviation between different frames and the RMI is independent from starting conditions and light exposure [57], thus permitting to obtain a realistic analysis of the mixing occurring in this device.

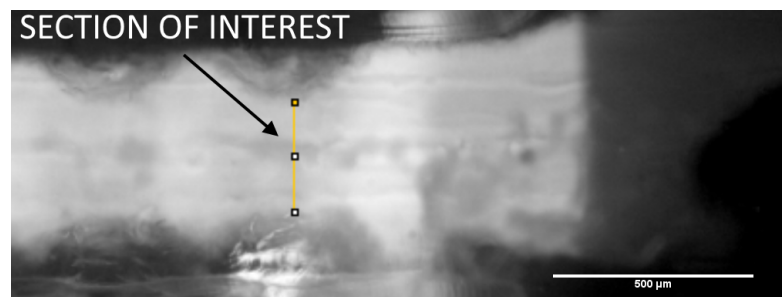


Figure 34: Section of interest, sidewall hemispheres design, constant flow rate.

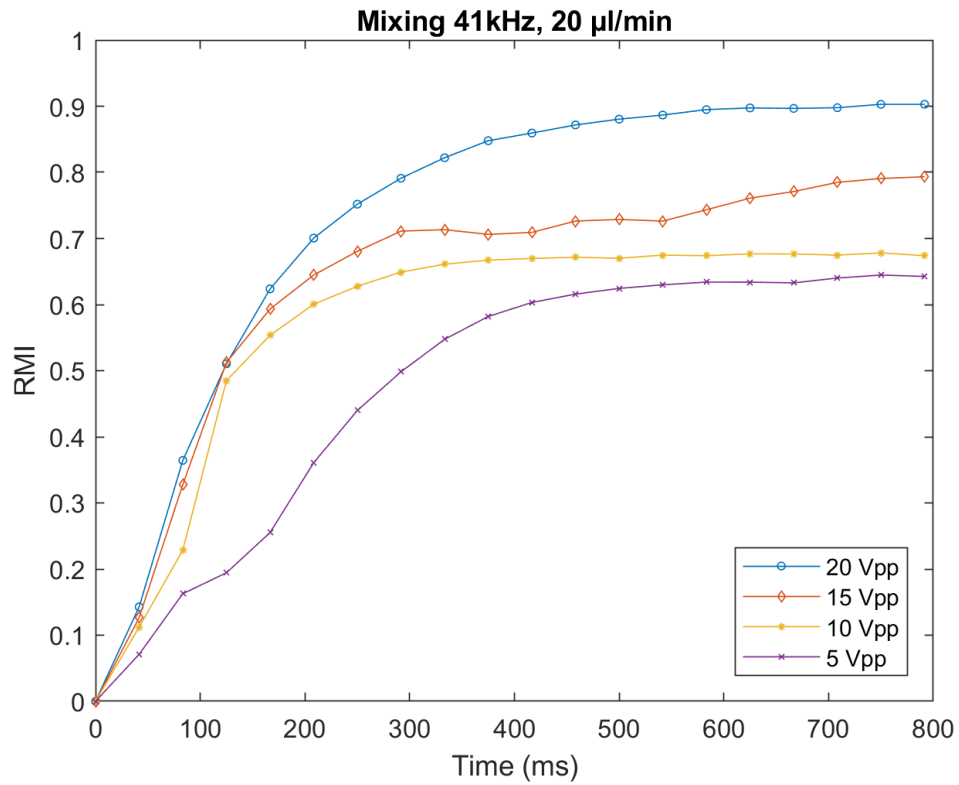


Figure 35: Mixing index as function of applied peak to peak voltage, sidewalls hemispheres design.

Figure 35 clearly shows the influence of the applied voltage on the relative mixing index. Notice that until around 120ms the response of the system is not highly affected by the voltage used, besides for the 5Vpp case. Generally, the mixing index tends to converge after around 400ms. Mixing at 20Vpp and 15 Vpp is extremely effective, thus confirming the initial hypothesis of mixing improvements by adding obstacles inside the channel. Figure 37 plots curves of

the RMI as function of the applied flow rate, at constant voltage. As noticeable in Figure 36, the device used for this test is different from the one use in Figure 34, since it broke after a series of experimental tests. Nevertheless this situation is exploited to test if the results are consistent between devices, since the 20Vpp - 20 μ l/min curve is shared in both tests. From Figure 37 it is possible to evince that two mixers made with the same design, due to slight chances in manufacturing or post-processing accuracy, have slightly different responses. The first one, which evidences a better accuracy, has a smoother response, while for the second the behavior is faster, but the mixing index reaches a lower value(0.823 vs 0.902) which introduces an uncertainty of the 8%. This discrepancy shows how defects in printing should be considered before designing microfluidic devices.

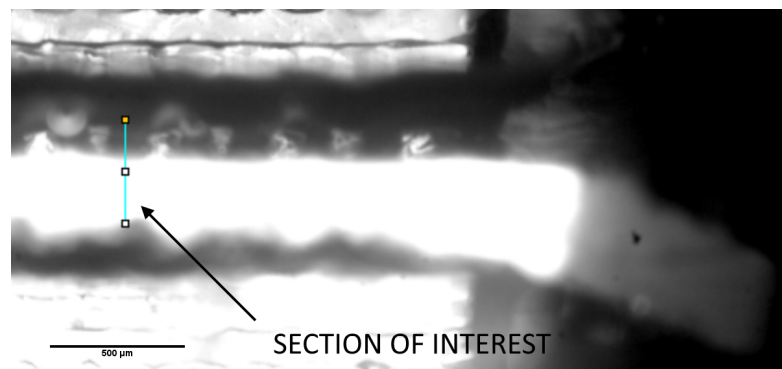


Figure 36: Section of interest, sidewall hemispheres design, constant peak to peak voltage.

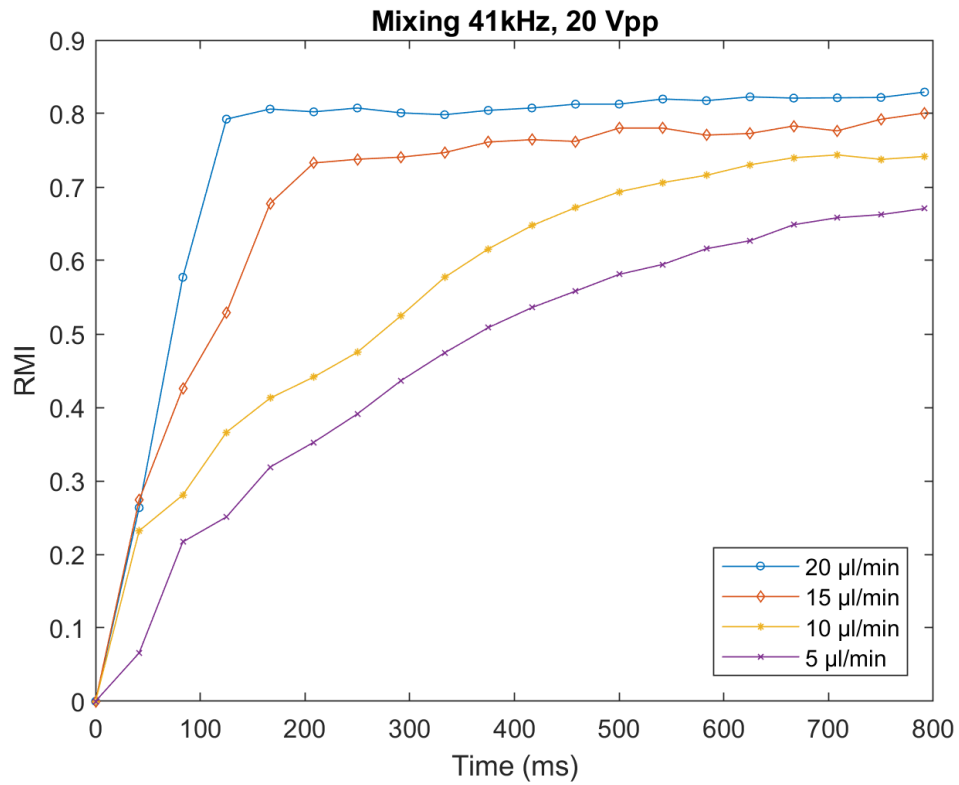


Figure 37: Mixing index as function of applied flow rate, sidewalls hemispheres design.

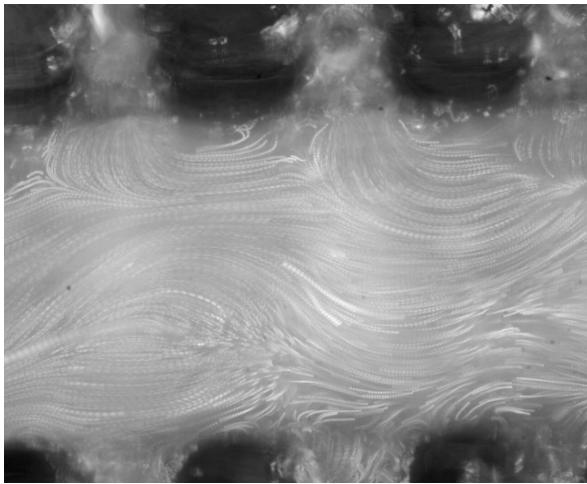
As expected the trend of the RMI is function of the applied flow rate, with lower velocities corresponding to smaller mixing indexes. Consider that mixing is quite efficient also for $5\mu\text{l}/\text{min}$.

4.4.3 Lateral channels design

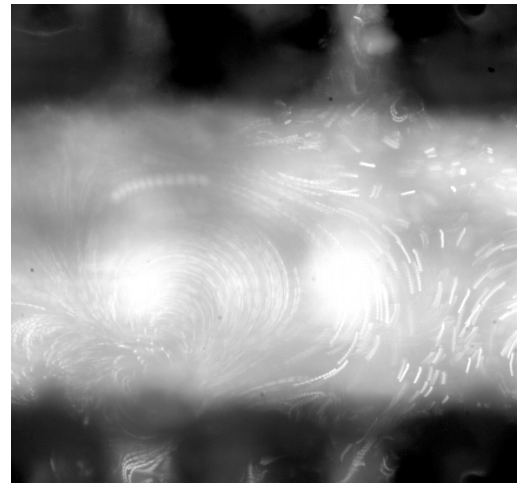
Concerning the lateral channels design it is necessary to stress out that tests have shown this concept to work, nevertheless various issues are still unsolved, which are mainly to be ascribed to the manufacturing and post-processing of the parts. Firstly, the device is able to run flow

rates up to $15\mu\text{l}/\text{min}$, higher values would produce leakages from the lateral channels. Secondly, top holes and sidewalls channels have different dimensions due to incomplete support material removal, therefore their working frequencies are not synchronized. Lateral channels start to produce mixing at 84 kHz, while little or no effect is shown at this frequency from the top channel holes. As for the other design, due to inaccuracies in printing, it is possible that certain holes do not show any influence on the flow. Moreover, microbubbles can remain trapped in the side channels, but generally they are not released into the main flow. At the current state of PolyJet technology is hard to think it could be possible to obtain better results. Ideally, leakages could be addressed using outward drafted channels, but an improved support removal system that does not damage the main holes should be used. The design and the results here presented are useful when dealing with very low flow rates (smaller than $15\mu\text{l}/\text{min}$) and should be considered as a proof of the current PolyJet printing state of the art for microchannel design and manufacturing.

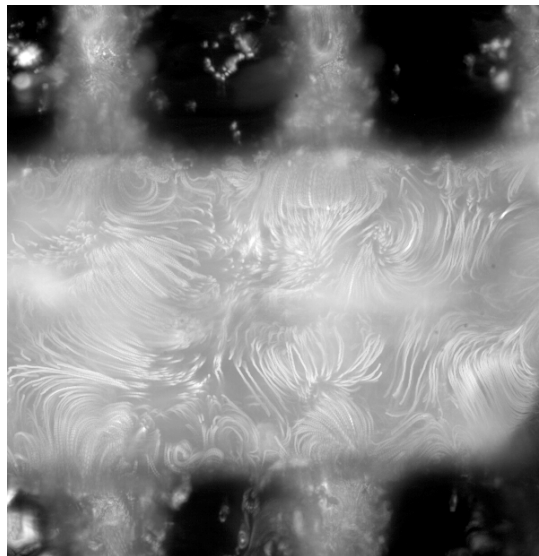
Figure 38 shows different microstreaming patterns, as found along different positions of the main microchannel (20x magnification, $4.8\mu\text{m}$ fluorescent beads). Figures (a-b) are obtained by an overlay of 30 frames, while figure (c) is a superimposition of 100 frames. The beads trajectories clearly explain the issues cited in the previous paragraph: microstreaming and mixing phenomena are present at 84kHz, although they are hardly controllable. Notice as microstreaming flow patterns are different and function of the channel geometries, consider also that channels are different one another and some are unable to induce a remarkable disturbance in the flow, like the top channels in Figure 38 (b).



(a)



(b)



(c)

Figure 38: Microstreaming patterns in sidewalls channels along different portion of a main microchannel. 20x enlargement. (a) 30 frames composition. (b) 30 frames composition. (c) 100 frames composition.

Figure 39 indicates the selected section for RMI evaluation for the lateral channels design. The average dimension for the lateral channels, indicated as point 1 in figure, is about $130\mu\text{m}$, therefore the holes evidence a strong deviation with respect to the 3D model dimensions.

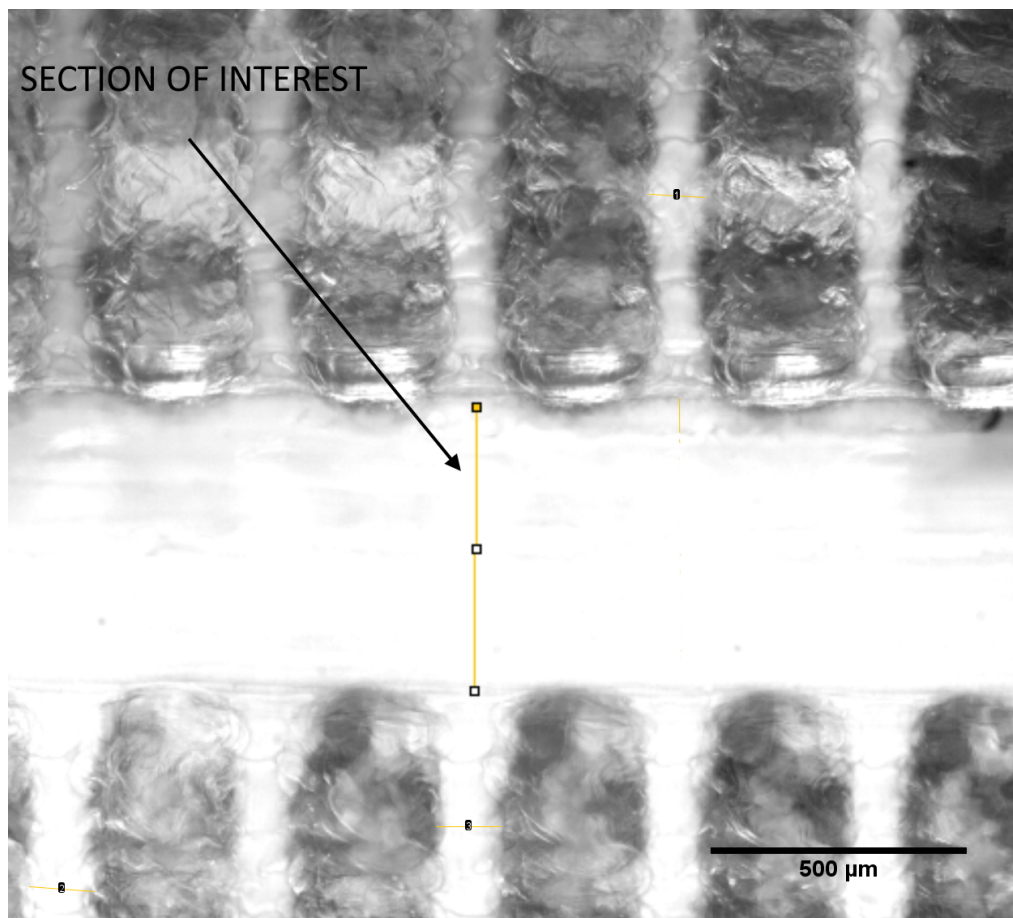


Figure 39: Section of interest, lateral channels design, constant flow rate. Notice section '1', which is used as reference to measure the dimension of a generic lateral channel.

Figure 40 shows the effect of voltage on the relative mixing index for the selected mixer. For this particular design the flow rate used for testing has been set to $15\mu\text{l}/\text{min}$, an higher value would produce leakages from the lateral channels.

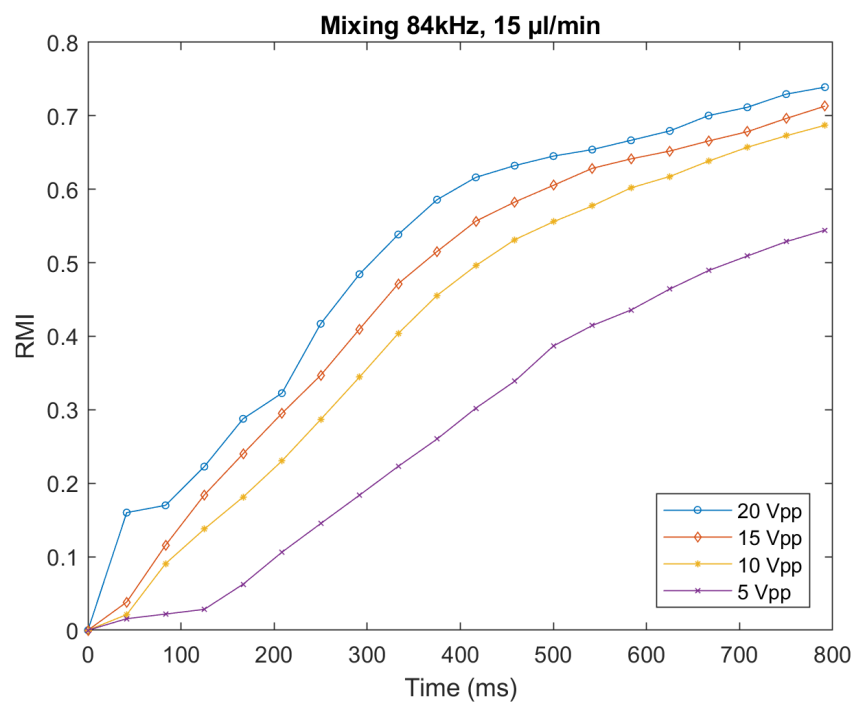


Figure 40: Mixing index as function of applied peak to peak voltage, lateral channels design.

Notice that it is still possible to obtain good and homogeneous mixing, nevertheless the time required is long, thus the device is unsuitable for all those applications in which good mixing is needed in a few hundred milliseconds. Microstreaming is produced by the superimposed

effects of liquid-air interface oscillations and bubbles vibrations inside lateral cavities. Mixing is effective after 400ms, voltages in the range 10-20 Vpp produce small variations in the device response. Maximum mixing index, here not shown in the plot, is 0.892 and it is reachable at 20Vpp for more than 2.25 seconds of continuous operation.

Figure 41 illustrates the effect of flow rate on the RMI in the cross section indicated in Figure 42.

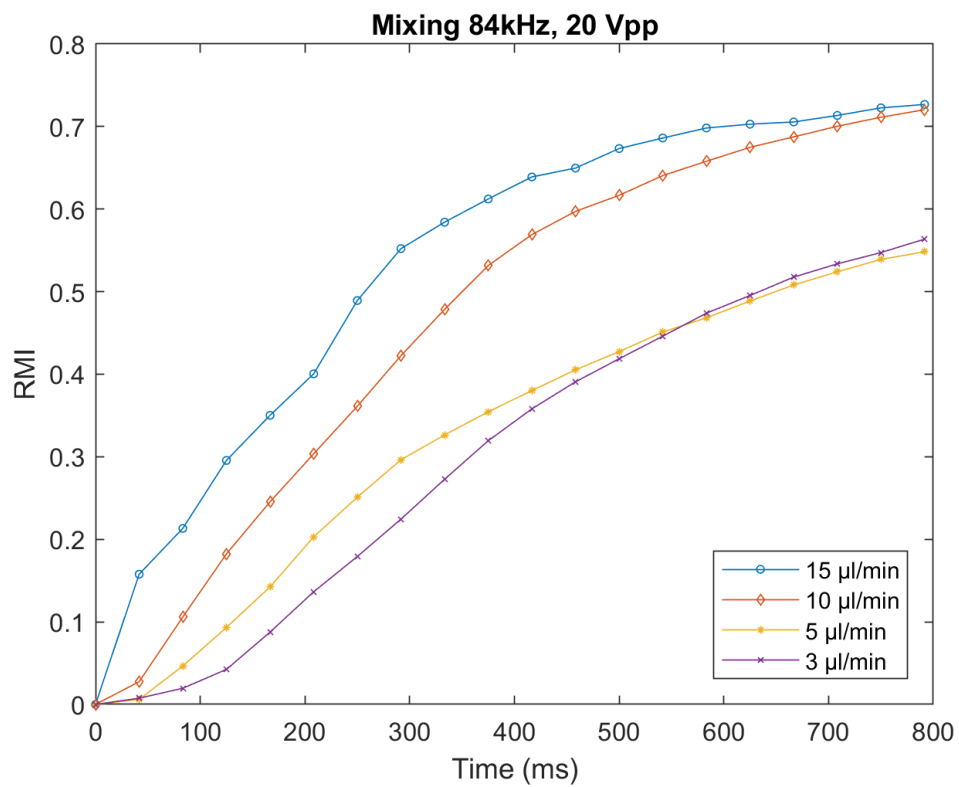


Figure 41: Mixing index as function of applied flow rate, lateral channels design.

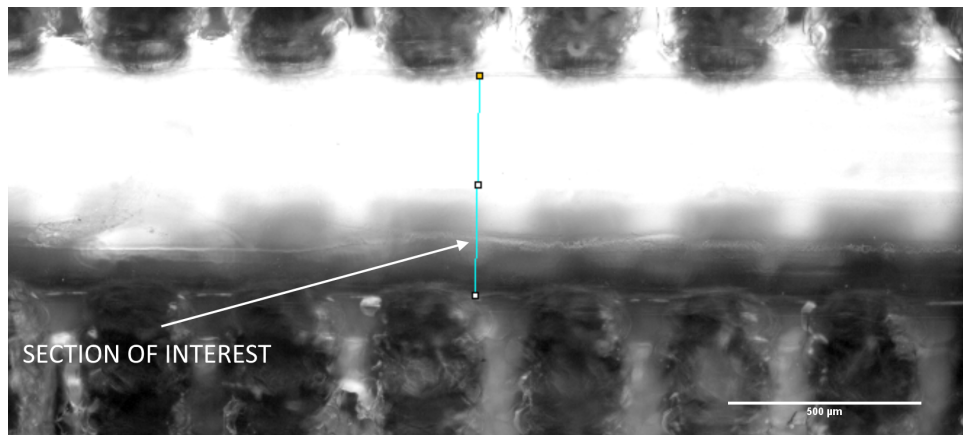


Figure 42: Cross section selected to evaluate RMI, case constant applied V_{pp} , lateral channels design.

Similarly to what shown in Figure 40, mixing is homogeneous for long time scales, while the rising time of the system is slow. Mixing at 5 and $3\mu\text{l}/\text{min}$ is extremely similar, this is shown by the superimposed trend of the two curves. Mixing curves at 10 and $15\mu\text{l}/\text{min}$ tend to superimpose from 600ms on, yielding practically the same relative mixing index. Notice that mixing is homogeneous, but it takes a long time to reach. Eventually a mixing index of about 0.84 is achieved, however elapsed time should be higher than 2.25 second, as shown in Figure 43 for a flow rate of $10\mu\text{l}/\text{min}$ at 20 V_{pp} . Usage of this mixer should be considered when low flow rates and slow, homogeneous mixing is required. Convergence trend is similar for all the mixer design (Figure 32). The curve in Figure 43 is obtained by linear interpolation of real data (shown as circles) extrapolated during experimental tests. Small oscillation of the RMI in the convergent part of the curve are due to the experimental nature of the analyzed data.

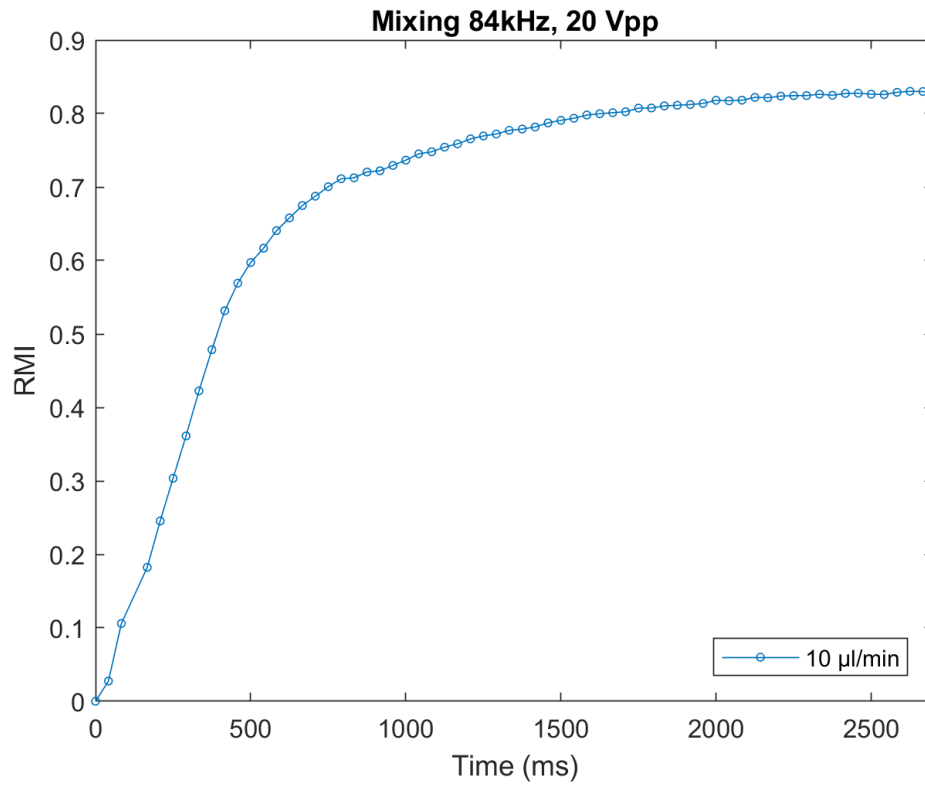


Figure 43: Convergence of relative mixing index, lateral channels design.

To conclude the subsection, consider images in Figure 44, where are shown two parts of a lateral channels mixers. Notice in (a) leakages taking place, while in (b) channels are filled by air. Notice that in case (b) it is hard to exactly control the amount of fluid filling the lateral channels. As shown in the pictures, in figure (b) support material in the lateral channels has been harder to remove, so at the interface with the main channel the lateral one are narrower, thus probably preventing the fluid to leak even at high flow rates.

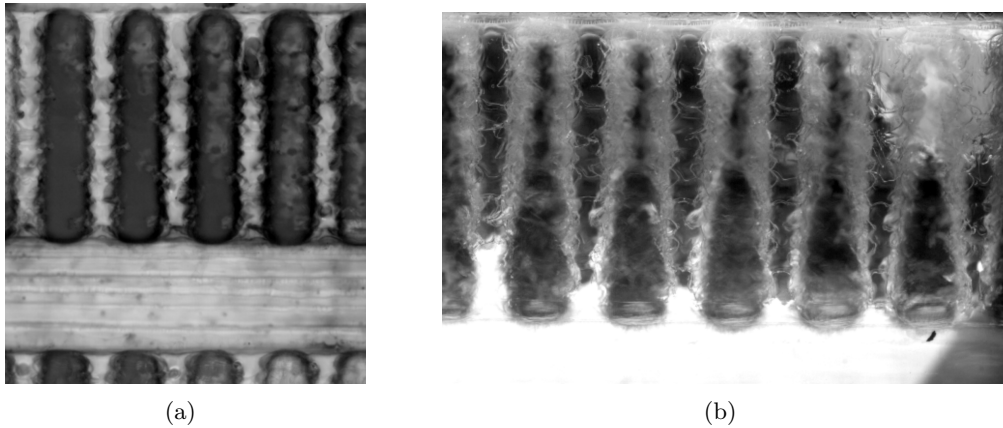


Figure 44: Lateral channels mixer. (a) Leakages in lateral channels. (b) Channels without leakages.

4.4.4 Design comparison

The sidewall hemisphere design and the basic design are interchangeable for flow rates higher than $15\mu\text{l}/\text{min}$, at fixed voltage. The response of the system at low time scale, in the range 0-100ms, is very similar, while the prior design produces slightly better mixing indexes in the converging part of the curve. At constant excitation voltage and low flow rates, the sidewalls hemispheres design achieves a consistently better RMI (Figure 37 and Figure 27).

The response of the basis design to a constant flow rate and a change in V_{pp} is sharper, nevertheless the sidewall hemispheres design produces a much better effects for times higher than 350ms. In particular the latter design yields a more homogeneous mixing at low applied voltages (Figure 27 and Figure 35.). Notice that results for the standard and sidewalls hemisphere designs have been calculated in similar cross sections.

Both designs shows a mixing index that tends to settle to a certain value for long time frames (Figure 32). A few holes could lead to such convergence, nevertheless more holes are suggested to guarantee correct functioning also if printing defects are present.

The lateral channels design shows a RMI trend that is something in between the two cases analyzed (Figure 40). Mixing is good, slightly better than the standard design, but also slightly lower than the one produced by the hemisphere mixer. Nevertheless, the response of the system is quite slow and a good RMI is obtainable only for long time scales (500ms on). Potentially the device could achieve an efficiency greater than 0.84 in mixing for high (15-20Vpp) applied voltages (Figure 43), but the time needed to yield the result ranges around 2.5s. In this regard, consider Figure 32 and Figure 43: both show the trend of RMI as function of the elapsed time. While the basic design reaches a stable values after a few hundreds of milliseconds, the lateral channel design needs about 2.5s to settle. Nevertheless in the latter case, mixing is more homogeneous. The devices should thus be used for different applications, according to mixing time and mixing efficiency needed.

The first two design can deal with flow rates up to $50\mu\text{l}/\text{min}$ without showing noticeable leakages, while the third design is limited to $15\mu\text{l}/\text{min}$. In all cases small leakages could arise in the first hole, as shown in Figure 45, which has been produced in all samples with the lowest dimensional accuracy and highest distortion. Probably issues are due to the fact the hole is positioned very closed to a change in thickness of the main body, at the connection with the Y-shaped region of the mixer. A design with the hole moved leftward is suggested.

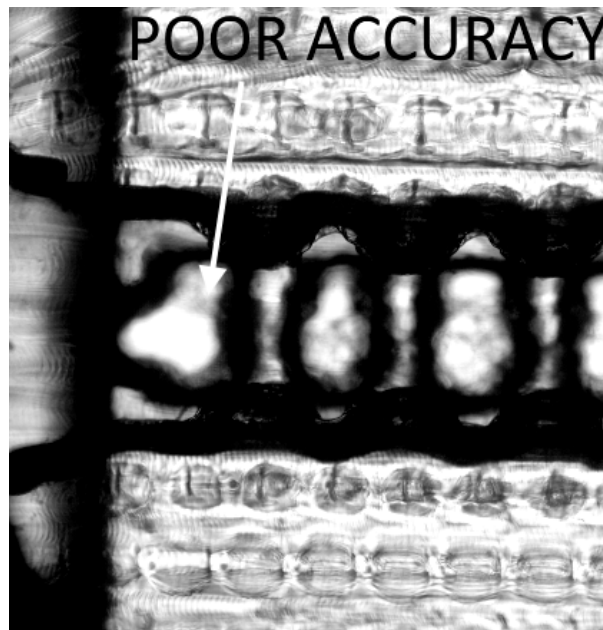


Figure 45: The picture show as the first hole in all batches for all 3 design has a very low dimensional accuracy.

It is important to stress out again that for the last design proposed its extremely hard to allow both lateral channels and top holes to work simultaneously at the same excitation frequency.

4.4.5 Final remarks and considerations

Three different micromixer design concepts have been proposed and tested, the basic and sidewall hemispheres design have proved to induce good and homogeneous mixing for different flow rates and applied peak to peak voltages. Anyhow, the third design shows some issues related to the manufacturing process and post-curing adopted. Devices can be easily customized to meet different demands in dimensions and geometry, it is though recommended to follow the

guidelines presented in section 3.2.4 to obtain optimal results. Shorter devices, with less holes, could be manufactured, since it has been proven in section 3.2.1 that 5 holes are enough to obtain good and homogeneous mixing, nevertheless, as shown in section 4.4.3, due to printing inaccuracies some holes could not work at the desired activation frequency, thus more cavities are suggested to be sure to obtain the needed RMI. Consider also, as indicated in section 4.4.2, that two devices printed with the same machine show similar but not exactly overlapping trends, which are due to small deviation in accuracy during printing. Induced errors are in the order of 8%. Eventually, experiments have shown that a few bubbles could be trapped into the main channel, especially if holes are printed with low accuracy, thus contributing to an improvement in the mixing efficiency. This issue should be taken into account prior to use, according to the requested application.

As already explained, clear pieces have been ordered and printed by a third producer, thus demonstrating how is potentially simple to design and rapidly obtain 3D printed microfluidic components. Ideally, even small labs that do not want to buy a 3D printed can conduce researches on the topic at low expenses, since each piece costs about 1\$ considering printing and shipping.

A final remark on 3D modelling should be made. It has been experienced that generally commercial CAD softwares do not allow for high level of customization when exporting the 3D design to a STL file for successive printing. Briefly, an STL file describes only the surfaces of a CAD file by means of a set of triangles [58]. The meshing process is essential to the printing process, poor SLT setting will lead to a rough model, in which the design is coarsely

approximated by the meshing pattern. Therefore, it is suggested to import the CAD file to AutoDesk Netfabb and use this software to export the STL. Netfabb allows the user to set custom tolerances on STL parameters, in particular on maximum surface deviation, angle and maximum edge length. Consider that lower the tolerance, higher will be the dimension of the final file. For small parts like the micromixers here presented, the final dimension are processed by the 3D printer software without any issues, but very large files could be hardly readable by a 3D printing slicer, thus it is recommended to set meshing is such a way to obtain a compromise between file weight and accuracy needed. Netfabb could also be useful to check the designed geometry for errors that could lead to defects in the STL export process. In this regard, the built in auto fixing tool could be very useful to quickly correct damaged STL.

CHAPTER 5

CONCLUSION

Three new active microfluidic mixers, manufactured by 3D printing, have been designed, fabricated and tested. Focus has been set on the suitability of PolyJet printing for microfluidic applications, in particular various manufacturing attempts have been made to assess the capabilities of the selected additive manufacturing technology.

It has been demonstrated that PolyJet printing is efficiently able to produce three dimensional, low cost devices for application in the microfluid field. Nevertheless, current state of the art PolyJet printers still have restrictions and limitations, which reduce design flexibility and manufacturing accuracy.

All the three micromixers have been proven to achieve a good and homogeneous mixing level, nevertheless settling time associated with high mixing indexes could be quite long, higher than 500ms. System response to acoustic waves is strong, however it is highly dependent on manufacturing accuracy and parts post-processing. Good mixing could be achieved with a few holes, especially at high applied peak to peak voltages.

The work has also permitted to prove the advantages and flexibility of 3D printing, in particular it has been shown that is easy to customize a design and print with a short lead time. Parts could also be ordered online and delivered in a couple of days, just sending an STL file to a third part manufacturer, thus allowing even small labs to obtain custom made 3D printed parts when needed. Point of care manufacturing is also feasible, although PolyJet

printers require a certain startup investment (starting from 19,000\$), which could be ten times higher respect to the cost of a standard desktop fused filament deposition or SLA machine [59].

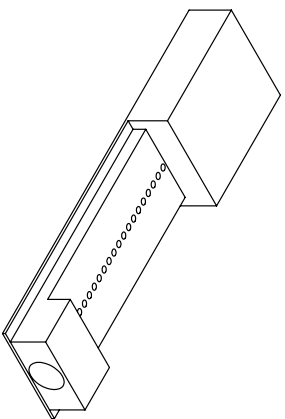
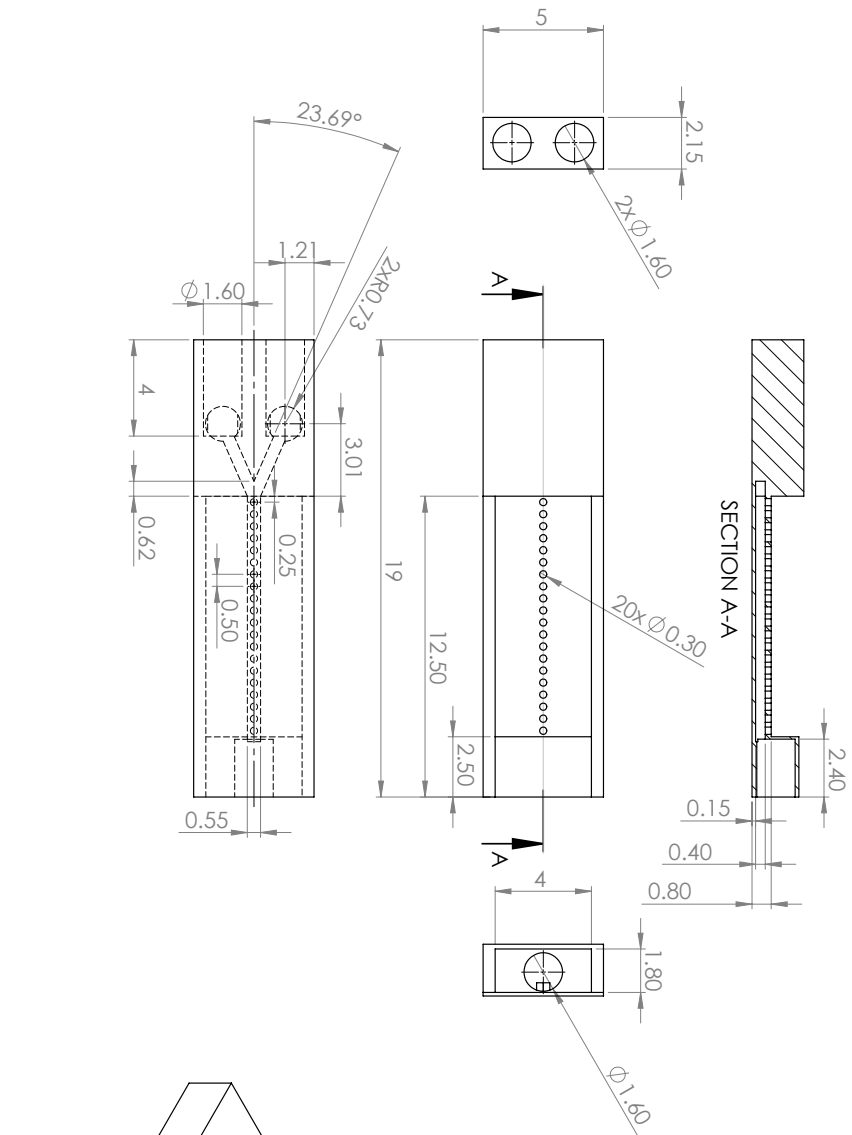
New, improved 3D printed microfluidic devices could be printed in a close future, as soon as new materials and machines are released to the market. It is also conceivable that the price of PolyJet printers would start to decrease, as soon the technology becomes more widespread, as happened with fused filament machines. More intricate architectures could possibly be allowed by MultiJet printers, considering that support material is removed by heat. Investigations should be performed in this direction.

Eventually, the development of a free online library containing 3D designs of standard microfluidic components could allow a further, fast improvement of the manufacturing technology, along with a more widespread use of microfluid devices in various engineering fields.

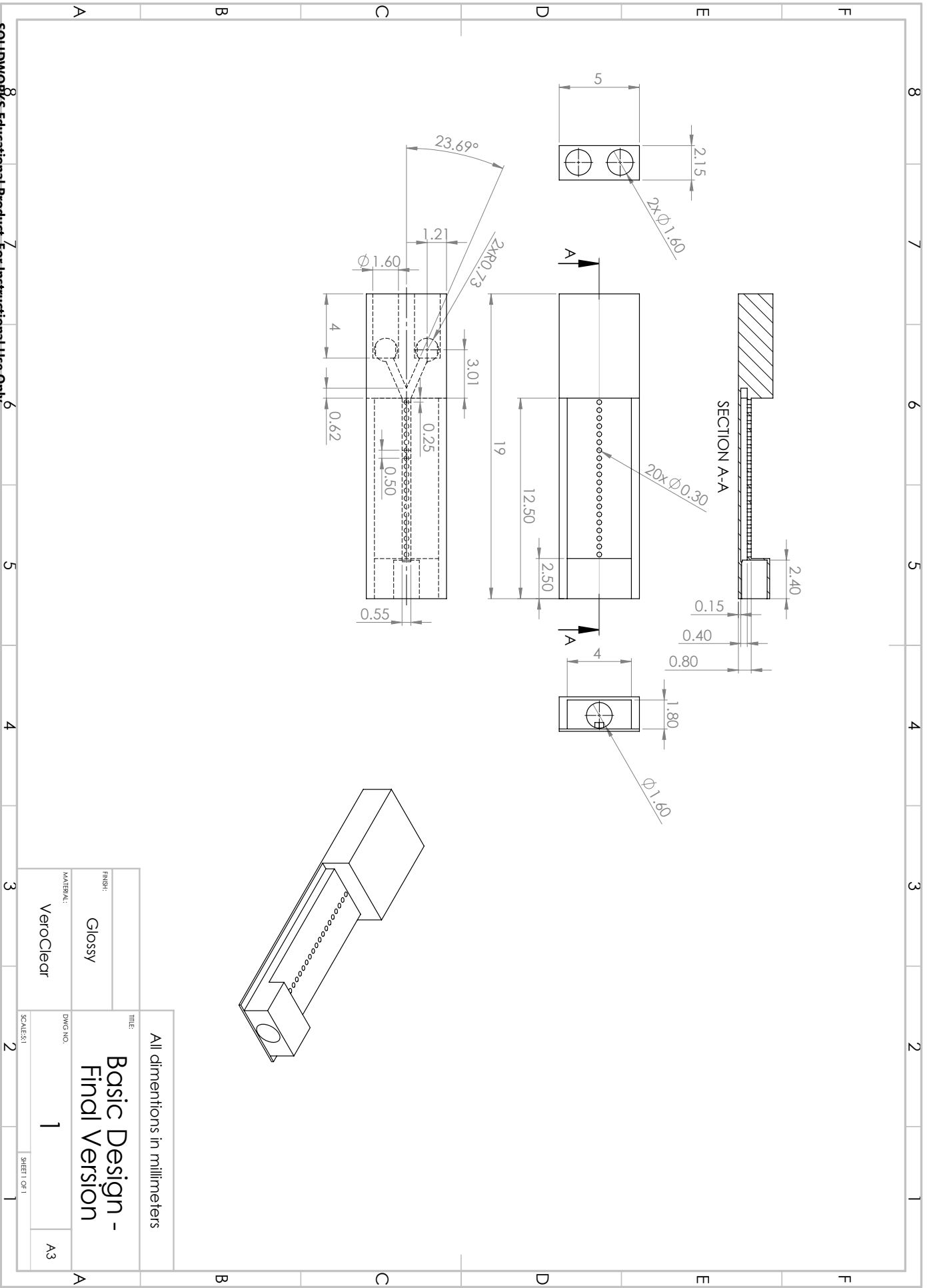
APPENDICES

Appendix A

ENGINEERING DRAWINGS - BASIC DESIGN

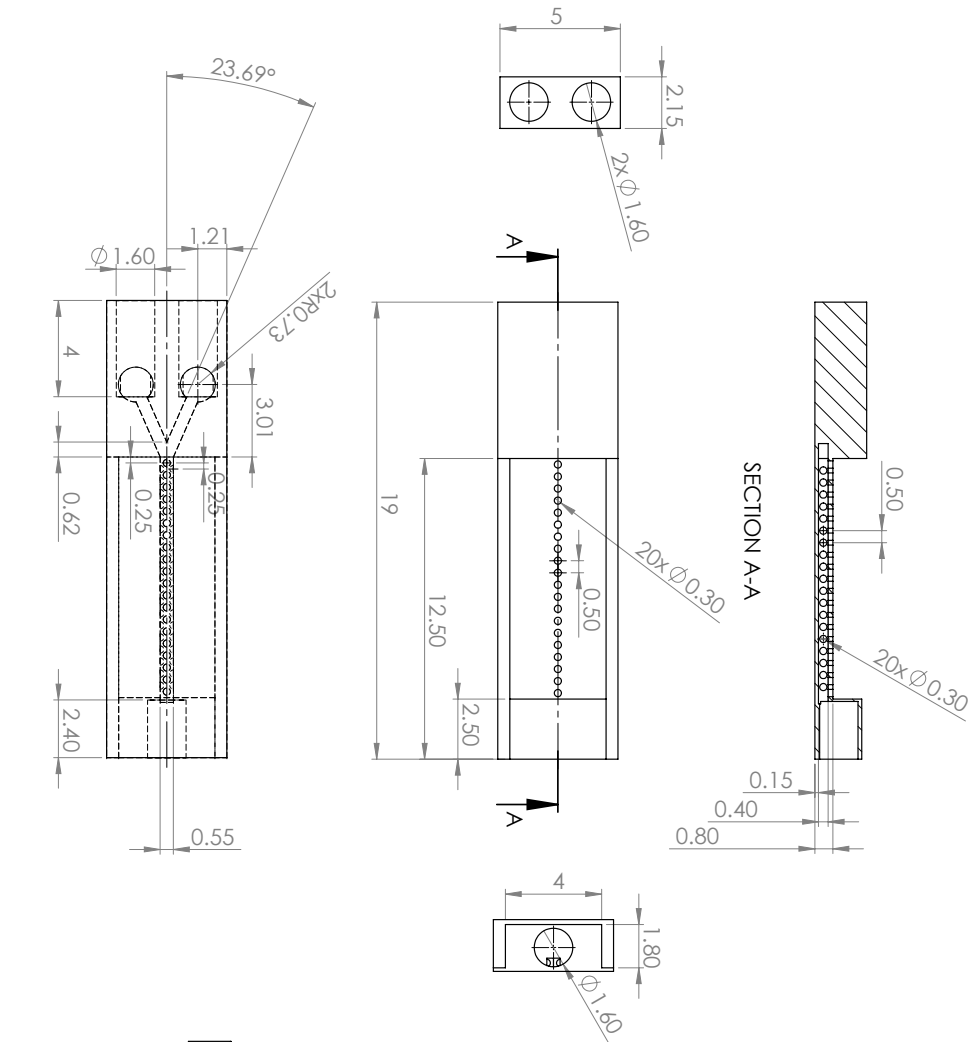


All dimensions in millimeters	
TITLE:	Basic Design - Final Version
FINISH:	Glossy
MATERIAL:	VeroClear
DWG NO.:	1
SCALE:	1
SHEET OF:	1
A3	



Appendix B

ENGINEERING DRAWINGS - SIDEWALLS HEMISPHERES DESIGN



All dimensions in millimeters

TITLE:
Sidewalls Hemispheres
Design - Final Version

FINISH:
Glossy

MATERIAL:
VeroClear

SCALE: 1

DWG. NO.:
2

SHEET 1 OF 1

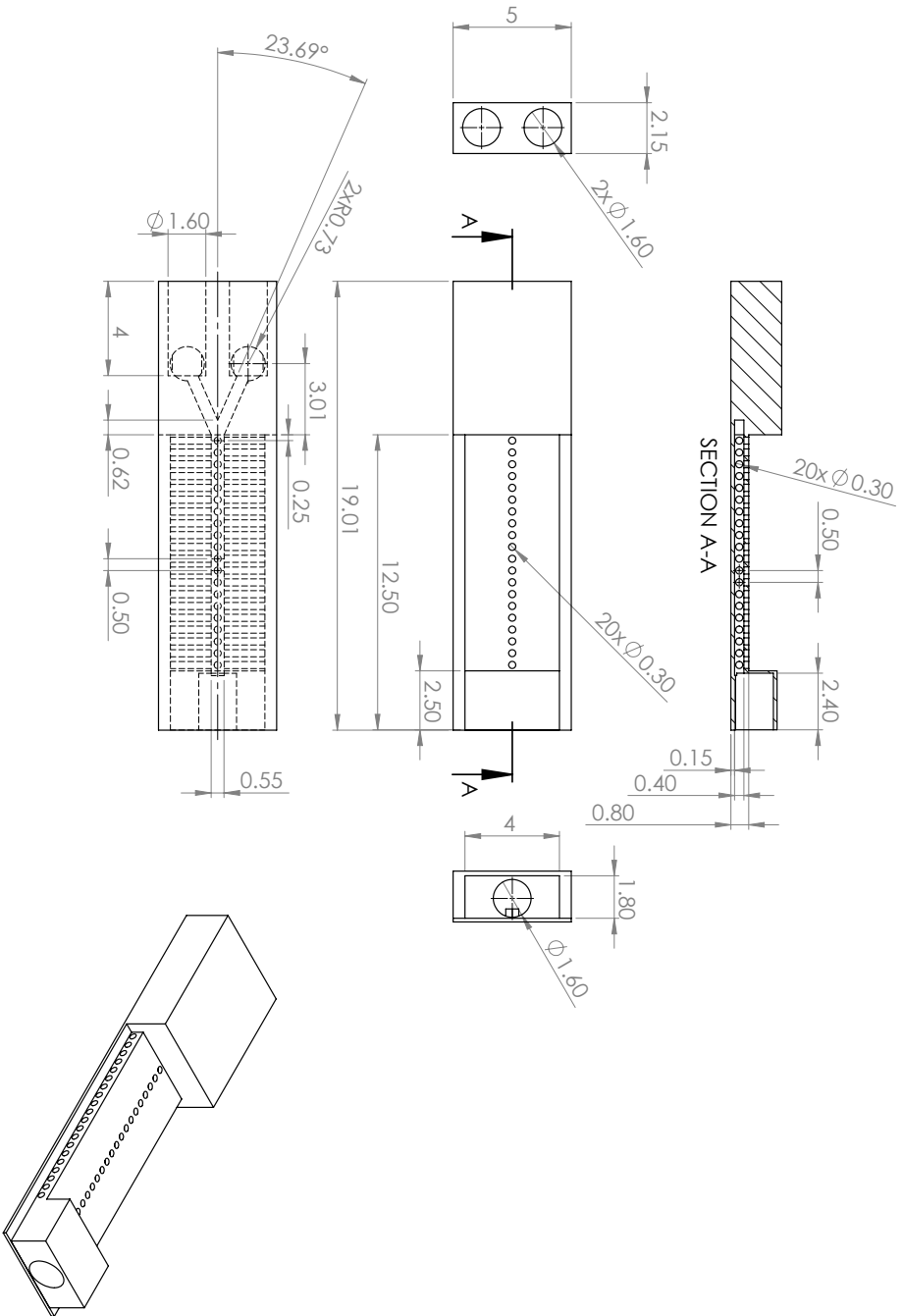
A3

8 7 6 5 4 3 2 1

A B C D E F

Appendix C

ENGINEERING DRAWINGS - LATERAL CHANNELS DESIGN



All dimintions in millimeters

TITLE
Lateral Channels Design
- Final Version

FINISH:
Glossy

MATERIAL:
VeroClear

DWG NO.:
3

SCALE: 1
SHEET 1 OF 1
A3

Appendix D

MATLAB SCRIPT - RMI CALCULATION

```
1 clear all
2
3 path=["C:\Users\princ\OneDrive\Desktop\Results20vpp.csv",
4       "C:\Users\princ\OneDrive\Desktop\Results15vpp.csv",
5       "C:\Users\princ\OneDrive\Desktop\Results10vpp.csv",
6       "C:\Users\princ\OneDrive\Desktop\Results5vpp.csv"
7       ]; %load files to be analyze
8
9 %Initialize time and RMI matrix, where 20 is the number of analyzed frames
10 time_matrix=zeros(20,length(path));
11 rmi_matrix=zeros(20,length(path));
12
13 for l=1:length(path)
14     results=xlsread(path(l,1)); %read one by one cvs with data
15     standard_dev=results(:,4); %get data on standard deviation
16     stack=results(:,8); %get data on frame used to calculate std
17
18     t_stack=1/24; %seconds elapsed between each frame
19     time=(stack*t_stack-stack(1)*t_stack)*1000;
20
```

Appendix D (continued)

```
21     std_zero=standard_dev(1,1); %get std in unmixed case
22     RMI=zeros(length(standard_dev)-1,1); %initiate RMI vector
23
24     for i=1:length(standard_dev)
25         RMI(i)=1-(standard_dev(i)/std_zero); %calculate RMI
26     end
27
28     time_matrix(:,1)=time;
29     rmi_matrix(:,1)=RMI;
30
31 end
32
33 %% Plot results
34 simbol=['o','d','*','x'];
35 for f=1:length(path)
36     p=plot(time_matrix(:,f),rmi_matrix(:,f))
37     hold on
38     xlabel('Time (ms)')
39     ylabel('RMI')
40     p.Marker=simbol(f);
41     p.MarkerSize=3;
42 end
43 legend({'20 Vpp','15 Vpp','10 Vpp','5 Vpp'},'Location','southeast')
44 title('Mixing 41kHz, 20 l/min')
```

Appendix E

EXAMPLE CSV FILE FROM IMAGEJ

	A	B	C	D	E	F	G	H	I	J
1		Label	Mean	StdDev	Min	Max	Angle	Slice	Length	
2	1	41khz_20v	196.2526	77.25228	57	255	-90	1291	85.33333	
3	2	41khz_20v	227.2635	59.32512	72	255	-90	1292	85.33333	
4	3	41khz_20v	229.7038	55.56024	77	255	-90	1293	85.33333	
5	4	41khz_20v	234.673	48.96327	85	255	-90	1294	85.33333	
6	5	41khz_20v	236.932	45.37511	94	255	-90	1295	85.33333	
7	6	41khz_20v	238.2872	43.15728	97	255	-90	1296	85.33333	
8	7	41khz_20v	239.4766	40.55187	105	255	-90	1297	85.33333	
9	8	41khz_20v	241.3032	36.71367	115	255	-90	1298	85.33333	
10	9	41khz_20v	243.1837	32.67562	122	255	-90	1299	85.33333	
11	10	41khz_20v	244.4119	29.68784	133	255	-90	1300	85.33333	
12	11	41khz_20v	245.4545	27.23333	139	255	-90	1301	85.33333	
13	12	41khz_20v	246.0841	25.33945	146	255	-90	1302	85.33333	
14	13	41khz_20v	246.6287	23.67564	153	255	-90	1303	85.33333	
15	14	41khz_20v	246.9763	22.70704	155	255	-90	1304	85.33333	
16	15	41khz_20v	247.4551	21.94415	156	255	-90	1305	85.33333	
17	16	41khz_20v	247.8607	20.83604	160	255	-90	1306	85.33333	
18	17	41khz_20v	248.1156	20.09147	163	255	-90	1307	85.33333	
19	18	41khz_20v	248.1852	19.80226	165	255	-90	1308	85.33333	
20	19	41khz_20v	248.1311	20.26614	165	255	-90	1309	85.33333	
21	20	41khz_20v	247.7643	19.96433	163	255	-90	1310	85.33333	
22										

Figure 46: Example of image analysis report from ImageJ. 20 frames are extracted to calculate the RMI, as seen in column A. Column B indicates the name of the saved video file, while column C to I give information on the selected cross section at the frame indicated under 'Slice'.

CITED LITERATURE

1. Fan, L.-L., Zhu, X.-L., Zhao, H., Zhe, J., and Zhao, L.: Rapid microfluidic mixer utilizing sharp corner structures. Microfluidics and Nanofluidics, 21(3):36, 2017.
2. Chen, K., Lu, H., Sun, M., Zhu, L., and Cui, Y.: Mixing enhancement of a novel c-sar microfluidic mixer. Chemical Engineering Research and Design, 132:338–345, 2018.
3. Lee, C.-Y., Chang, C.-L., Wang, Y.-N., and Fu, L.-M.: Microfluidic mixing: a review. International journal of molecular sciences, 12(5):3263–3287, 2011.
4. Ward, K. and Fan, Z. H.: Mixing in microfluidic devices and enhancement methods. Journal of Micromechanics and Microengineering, 25(9):094001, 2015.
5. Chen, C., Mehl, B. T., Munshi, A. S., Townsend, A. D., Spence, D. M., and Martin, R. S.: 3d-printed microfluidic devices: fabrication, advantages and limitations a mini review. Analytical Methods, 8(31):6005–6012, 2016.
6. Au, A. K., Huynh, W., Horowitz, L. F., and Folch, A.: 3d-printed microfluidics. Angewandte Chemie International Edition, 55(12):3862–3881, 2016.
7. Liu, M., Han, X., Cao, Q., and Li, L.: Performance analysis of a microfluidic mixer based on high gradient magnetic separation principles. Journal of Physics D: Applied Physics, 50(36):365004, 2017.
8. Xia, H., Wan, S., Shu, C., and Chew, Y.: Chaotic micromixers using two-layer crossing channels to exhibit fast mixing at low reynolds numbers. Lab on a Chip, 5(7):748–755, 2005.
9. Buchegger, W., Wagner, C., Lendl, B., Kraft, M., and Vellekoop, M. J.: A highly uniform lamination micromixer with wedge shaped inlet channels for time resolved infrared spectroscopy. Microfluidics and Nanofluidics, 10(4):889–897, 2011.
10. Wang, W., Zhao, S., Shao, T., Jin, Y., and Cheng, Y.: Visualization of micro-scale mixing in miscible liquids using μ -lif technique and drug nano-particle preparation in t-shaped micro-channels. Chemical engineering journal, 192:252–261, 2012.

CITED LITERATURE (continued)

11. Hsieh, S.-S., Lin, J.-W., and Chen, J.-H.: Mixing efficiency of y-type micromixers with different angles. International Journal of Heat and Fluid Flow, 44:130–139, 2013.
12. Glasgow, I. and Aubry, N.: Enhancement of microfluidic mixing using time pulsing. Lab on a Chip, 3(2):114–120, 2003.
13. Yang, Z., Matsumoto, S., Goto, H., Matsumoto, M., and Maeda, R.: Ultrasonic micromixer for microfluidic systems. Sensors and Actuators A: Physical, 93(3):266–272, 2001.
14. Lu, L.-H., Ryu, K. S., and Liu, C.: A novel microstirrer and arrays for microfluidic mixing. In Micro Total Analysis Systems 2001, pages 28–30. Springer, 2001.
15. Ahmed, D., Mao, X., Juluri, B. K., and Huang, T. J.: A fast microfluidic mixer based on acoustically driven sidewall-trapped microbubbles. Microfluidics and nanofluidics, 7(5):727, 2009.
16. Bhargava, K. C., Ermagan, R., Thompson, B., Friedman, A., and Malmstadt, N.: Modular, discrete micromixer elements fabricated by 3d printing. Micromachines, 8(5):137, 2017.
17. Amin, R., Knowlton, S., Hart, A., Yenilmez, B., Ghaderinezhad, F., Katebifar, S., Messina, M., Khademhosseini, A., and Tasoglu, S.: 3d-printed microfluidic devices. Biofabrication, 8(2):022001, 2016.
18. Bhargava, K. C., Thompson, B., and Malmstadt, N.: Discrete elements for 3d microfluidics. Proceedings of the National Academy of Sciences, 111(42):15013–15018, 2014.
19. Chen, Y., Fang, Z., Merritt, B., Strack, D., Xu, J., and Lee, S.: Onset of particle trapping and release via acoustic bubbles. Lab on a Chip, 16(16):3024–3032, 2016.
20. Hashmi, A., Yu, G., Reilly-Collette, M., Heiman, G., and Xu, J.: Oscillating bubbles: a versatile tool for lab on a chip applications. Lab on a Chip, 12(21):4216–4227, 2012.
21. Liu, R. H., Yang, J., Pindera, M. Z., Athavale, M., and Grodzinski, P.: Bubble-induced acoustic micromixing. Lab on a Chip, 2(3):151–157, 2002.
22. Chung, S. K. and Cho, S. K.: On-chip manipulation of objects using mobile oscillating bubbles. Journal of Micromechanics and Microengineering, 18(12):125024, 2008.

CITED LITERATURE (continued)

23. Xu, J. and Attinger, D.: Piezoelectric actuation in multiphase microfluidics. Encyclopedia of Microfluidics and Nanofluidics, pages 2735–2743, 2015.
24. Tovar, A. R. and Lee, A. P.: Lateral cavity acoustic transducer. Lab on a Chip, 9(1):41–43, 2009.
25. Garg, N., Vallejo, D., Boyle, D., Nanayakkara, I., Teng, A., Pablo, J., Liang, X., Camerini, D., Lee, A., and Felgner, P.: Integrated on-chip microfluidic immunoassay for rapid biomarker detection. Procedia engineering, 159:53–57, 2016.
26. Bertsch, A., Heimgartner, S., Cousseau, P., and Renaud, P.: 3d micromixers-downscaling large scale industrial static mixers. In Micro Electro Mechanical Systems, 2001. MEMS 2001. The 14th IEEE International Conference on, pages 507–510. IEEE, 2001.
27. Bonyár, A., Sántha, H., Ring, B., Varga, M., Kovács, J. G., and Harsányi, G.: 3d rapid prototyping technology (rpt) as a powerful tool in microfluidic development. Procedia Engineering, 5:291–294, 2010.
28. Bishop, G. W., Satterwhite, J. E., Bhakta, S., Kadimisetty, K., Gillette, K. M., Chen, E., and Rusling, J. F.: 3d-printed fluidic devices for nanoparticle preparation and flow-injection amperometry using integrated prussian blue nanoparticle-modified electrodes. Analytical chemistry, 87(10):5437–5443, 2015.
29. Shallan, A. I., Smejkal, P., Corban, M., Guijt, R. M., and Breadmore, M. C.: Cost-effective three-dimensional printing of visibly transparent microchips within minutes. Analytical chemistry, 86(6):3124–3130, 2014.
30. Nie, J., Gao, Q., Qiu, J.-j., Sun, M., Liu, A., Shao, L., Fu, J.-z., Zhao, P., and He, Y.: 3d printed lego®-like modular microfluidic devices based on capillary driving. Biofabrication, 10(3):035001, 2018.
31. Soe, A. K., Fielding, M., and Nahavandi, S.: Lab-on-a-chip turns soft: Computer-aided, software-enabled microfluidics design. In Advances in Social Networks Analysis and Mining (ASONAM), 2013 IEEE/ACM International Conference on, pages 968–971. IEEE, 2013.
32. Elveflow: INTRODUCTION ABOUT PDMS SOFT-LITHOGRAPHY AND POLYMER MOLDING FOR MICROFLUIDICS. <https://www.elveflow.com/microfluidic-tutorials/soft-lithography-reviews-and-tutorials/>

CITED LITERATURE (continued)

- introduction-about-soft-lithography-and-polymer-molding-for-microfluidic/, [Online, accessed on 04-04-2018].
33. Wikipedia: 3D Printing. https://en.wikipedia.org/wiki/3D_printing, [Online, accessed on 04-04-2018].
 34. 3DHUBS: What is 3D Printing? The definitive guide to additive manufacturing. <https://www.3dhubs.com/what-is-3d-printing>, [Online, accessed on 04-04-2018].
 35. Waheed, S., Cabot, J. M., Macdonald, N. P., Lewis, T., Guijt, R. M., Paull, B., and Breadmore, M. C.: 3d printed microfluidic devices: enablers and barriers. Lab on a Chip, 16(11):1993–2013, 2016.
 36. 3DHUBS: Introduction to SLA 3D Printing. <https://www.3dhubs.com/knowledge-base/introduction-sla-3d-printing>, [Online, accessed on 04-04-2018].
 37. Formlabs, Inc: Form 2: Desktop Stereolithography (SLA) 3D printer. <https://formlabs.com/3d-printers/form-2/>, [Online, accessed on 04-04-2018].
 38. 3D Systems, Inc: Pro X 950. <https://www.3dsystems.com/3d-printers/prox-950>, [Online, accessed on 04-04-2018].
 39. Nanoscribe GmbH: Nanoscribe. <https://www.nanoscribe.de/en/>, [Online, accessed on 04-04-2018].
 40. 3DHUBS: Introduction to Material Jetting 3D Printing. <https://www.3dhubs.com/knowledge-base/introduction-material-jetting-3d-printing>, [Online, accessed on 04-04-2018].
 41. Stratasys Ltd.: Objet Eden260VS. <http://www.stratasys.com/3d-printers/objet-eden260vsy>, [Online, accessed on 04-04-2018].
 42. MASTERGRAPHICS: Multi Jet And Poly Jet Post Processing. <http://mastergraphics.com/blog/multi-jet-and-poly-jet-post-processing/>, [Online, accessed on 04-05-2018].
 43. Stratasys Ltd.: Vero. <http://www.stratasys.com/materials/search/vero>, [Online, accessed on 04-15-2018].

CITED LITERATURE (continued)

44. Stratasys Ltd.: RGD720. <http://www.stratasys.com/materials/search/rgd720>, [Online, accessed on 04-15-2018].
45. Bachman, H., Huang, P.-H., Zhao, S., Yang, S., Zhang, P., Fu, H., and Huang, T. J.: Acoustofluidic devices controlled by cell phones. Lab on a Chip, 2018.
46. Tofteberg, T., Skolimowski, M., Andreassen, E., and Geschke, O.: A novel passive micromixer: lamination in a planar channel system. Microfluidics and Nanofluidics, 8(2):209–215, 2010.
47. Tovar, A. R. and Lee, A. P.: Lateral cavity acoustic transducer. Lab on a Chip, 9(1):41–43, 2009.
48. Ahmed, D., Muddana, H. S., Lu, M., French, J. B., Ozcelik, A., Fang, Y., Butler, P. J., Benkovic, S. J., Manz, A., and Huang, T. J.: Acoustofluidic chemical waveform generator and switch. Analytical chemistry, 86(23):11803–11810, 2014.
49. SyringePumpPro : Chemyx - SyringePumpPro . <https://syringepumppro.com/chemyx/>, [Online, accessed on 04-22-2018].
50. NIKON INSTRUMENTS INC.: Eclipse Ti-U. <https://www.nikoninstruments.com/Products/Inverted-Microscopes/Eclipse-Ti-U>, [Online, accessed on 04-22-2018].
51. Amazon: Owfeel 60W 40KHz Ultrasound Transducer Ultrasonic Piezoelectric Transducer Cleaner. <https://www.amazon.co.uk/Owfeel-Ultrasound-Transducer-Ultrasonic-Piezoelectric/dp/B00QF9HP90>, [Online, accessed on 04-22-2018].
52. RIGOL Technologies Inc.: DG1000 SERIES — ARBITRARY WAVEFORM FUNCTION GENERATORS. <https://www.rigolna.com/products/waveform-generators/dg1000/>, [Online, accessed on 04-22-2018].
53. TEGAM Inc.: Product Categories Waveform Amplifiers Archive. <https://www.tegam.com/product-category/signal-source-amplifier/waveform-amplifiers/>, [Online, accessed on 04-22-2018].
54. Wikipedia: Reynolds Number. https://en.wikipedia.org/wiki/Reynolds_number, [Online, accessed on 04-04-2018].

CITED LITERATURE (continued)

55. Hessel, V., Löwe, H., and Schönfeld, F.: Micromixers: a review on passive and active mixing principles. Chemical Engineering Science, 60(8-9):2479–2501, 2005.
56. Liu, R. H., Stremler, M. A., Sharp, K. V., Olsen, M. G., Santiago, J. G., Adrian, R. J., Aref, H., and Beebe, D. J.: Passive mixing in a three-dimensional serpentine microchannel. Journal of microelectromechanical systems, 9(2):190–197, 2000.
57. Hashmi, A. and Xu, J.: On the quantification of mixing in microfluidics. Journal of laboratory automation, 19(5):488–491, 2014.
58. Wikipedia: STL (file format). [https://en.wikipedia.org/wiki/STL_\(file_format\)](https://en.wikipedia.org/wiki/STL_(file_format)), [Online, accessed on 04-22-2018].
59. 3DHUBS: 3D Printer Index. <https://www.3dhubs.com/3d-printers>, [Online, accessed on 04-22-2018].
60. MGSC: What is PolyJet? <https://www.gsc-3d.com/articles/2017/11/what-polyjet-3d-printing-technology/>, [Online, accessed on 04-04-2018].

VITA

NAME	Matteo Tamone
<hr/>	
EDUCATION	
	Master of Science in Mechanical Engineering, University of Illinois at Chicago, May 2018, USA
	Bachelor's Degree in Mechanical Engineering, Oct 2016, Polytechnic of Turin, Italy
<hr/>	
LANGUAGE SKILLS	
Italian	Native speaker
English	Full working proficiency
	2017 - IELTS examination, 7.5 Overall Score
	A.Y. 2017/18 One year of study abroad in Chicago, Illinois
	Bachelor and Master lessons and exams attended exclusively in English
<hr/>	
SCHOLARSHIPS	
2017	Italian scholarship for TOP-UIC students
<hr/>	
TECHNICAL SKILLS	
Programming	C, Python
Software	SolidWorks, Matlab, Simulink, Microsoft Word, Excel, PowerPoint, AutoCad, LaTeX
Hardware	Arduino microcontroller
ACADEMIC PROJECTS	
Fall 2017 -	Digital implementation and hardware in the loop simulation PID controller. Designed input-output interface of a proportional-integral-derivative (PID) controller for hardware in the loop simulation and testing, using Arduino board. Implementation of the control logic by means of Simulink and Arduino integrated development environment (IDE).

VITA (continued)

Matlab Monte Carlo simulation of a truss structure. Matlab implementation of an algorithm to simulate by Montecarlo technique the displacement of a truss structure having Gaussian distributed elastic moduli.

Passive and active circuit design and testing. Design and testing of passive/active low, high, band and notch pass filters. Design and testing of analog proportional- integral-derivative controller.

Spring 2017 -

Matlab - Variation of temperature in a hot water tank. Simulated evolution of temperature profile inside a hot water storage tank connected to solar collectors by means of a Matlab finite elements toolbox.

Machine Design Speed increaser analysis and design. Performed static and fatigue analysis (FKM standard) of a speed increaser connected to a Kaplan turbine. Bearing life testing under different loading conditions. SolidWorks shaft/bearing assembly. Definition of gear geometry and root-strength/tooth surface fatigue calculation (DIN standard). Design, dimensioning and tolerancing (GD&T) of mechanical component

Fall 2016 -

Gearbox design and verification. Design of a simple dual stage gearbox by means of analytical formulas (reference Shigleys Mechanical Engineering Design). Static (Tresca) and fatigue verification (Haigh diagram) of shafts. Bearing selection from SKF catalogue, rating life calculation. SolidWorks modeling of shafts and assemblies
